J Neurophysiol 116: 2312–2330, 2016.
First published August 17, 2016; doi:10.1152/jn.00318.2016.

Large-scale recording of thalamocortical circuits: in vivo electrophysiology with the two-dimensional electronic depth control silicon probe

Richárd Fiáth,[1,2,3] Patrícia Beregszászi,[2] Domonkos Horváth,[1,2,3] Lucia Wittner,[1] Arno A. A. Aarts,[4] Patrick Ruther,[5,6] Hercules P. Neves,[7,8] Hajnalka Bokor,[9] László Acsády,[9] and István Ulbert[1,2]

[1]*Group of Comparative Psychophysiology, Institute of Cognitive Neuroscience and Psychology, Research Centre for Natural Sciences, Hungarian Academy of Sciences, Budapest, Hungary;* [2]*Faculty of Information Technology and Bionics, Pázmány Péter, Catholic University, Budapest, Hungary;* [3]*School of Ph.D. Studies, Semmelweis University, Budapest, Hungary;* [4]*ATLAS NeuroEngineering, Leuven, Belgium;* [5]*Department of Microsystems Engineering (IMTEK), University of Freiburg, Freiburg, Germany;* [6]*BrainLinks-BrainTools Cluster of Excellence, University of Freiburg, Freiburg, Germany;* [7]*Unitec Semicondutores, Ribeirão das Neves, Brazil;* [8]*Solid State Electronics, Department of Engineering Sciences, Uppsala University, Uppsala, Sweden; and* [9]*Laboratory of Thalamus Research, Institute of Experimental Medicine, Hungarian Academy of Sciences, Budapest, Hungary*

Submitted 21 April 2016; accepted in final form 13 August 2016

Fiáth R, Beregszászi P, Horváth D, Wittner L, Aarts AA, Ruther P, Neves HP, Bokor H, Acsády L, Ulbert I. Large-scale recording of thalamocortical circuits: in vivo electrophysiology with the two-dimensional electronic depth control silicon probe. *J Neurophysiol* 116: 2312–2330, 2016. First published August 17, 2016; doi:10.1152/jn.00318.2016.—Recording simultaneous activity of a large number of neurons in distributed neuronal networks is crucial to understand higher order brain functions. We demonstrate the in vivo performance of a recently developed electrophysiological recording system comprising a two-dimensional, multi-shank, high-density silicon probe with integrated complementary metal-oxide semiconductor electronics. The system implements the concept of electronic depth control (EDC), which enables the electronic selection of a limited number of recording sites on each of the probe shafts. This innovative feature of the system permits simultaneous recording of local field potentials (LFP) and single- and multiple-unit activity (SUA and MUA, respectively) from multiple brain sites with high quality and without the actual physical movement of the probe. To evaluate the in vivo recording capabilities of the EDC probe, we recorded LFP, MUA, and SUA in acute experiments from cortical and thalamic brain areas of anesthetized rats and mice. The advantages of large-scale recording with the EDC probe are illustrated by investigating the spatiotemporal dynamics of pharmacologically induced thalamocortical slow-wave activity in rats and by the two-dimensional tonotopic mapping of the auditory thalamus. In mice, spatial distribution of thalamic responses to optogenetic stimulation of the neocortex was examined. Utilizing the benefits of the EDC system may result in a higher yield of useful data from a single experiment compared with traditional passive multielectrode arrays, and thus in the reduction of animals needed for a research study.

electronic depth control; silicon probe; high-density recording; thalamocortical oscillation; optogenetics

NEW & NOTEWORTHY

Recording the electrical activity of a large number of neurons located in the thalamocortical network is a prerequisite for the understanding of mechanism underlying higher order brain functions. We verified the in vivo performance of an innovative electrophysiological recording system that allows the electronic selection of recording sites on multi-shank, high-density, silicon-based probes. This approach is well-suited to record local field potentials and multiple- and single-unit activity from spatially distinct brain areas of anesthetized rodents.

DESPITE THE RAPID ADVANCEMENT of brain imaging techniques offering both high spatial and temporal resolution, electrophysiological tools are still widely used methods to investigate the complex spatiotemporal activity patterns of neuronal circuits. Over the past few decades, single-wire electrodes used for in vivo extracellular recording of action potentials evolved into multielectrode arrays covering the range of up to 1,000 recording sites (Bai and Wise 2001; Berényi et al. 2014; Blanche et al. 2005; Bragin et al. 2000; Campbell et al. 1991; Chen et al. 2009; Cheung 2007; Csicsvari et al. 2003; Drake et al. 1988; Du et al. 2009, 2011; Grand et al. 2011; Karmos et al. 1982; Khodagholy et al. 2015; Kipke et al. 2008; Kubie 1984; Lopez et al. 2014; Márton et al. 2015; McNaughton et al. 1983; Michon et al. 2016; Okeefe and Recce 1993; Ruther et al. 2010; Ruther and Paul 2015; Scholvin et al. 2016; Seidl et al. 2011, 2012; Shobe et al. 2015; Torfs et al. 2011; Wilson and McNaughton 1993; Wise et al. 1970, 2008). With such a high number of recording sites neuroscientists are able to monitor the activity of hundreds of neurons simultaneously both in anesthetized and in freely moving animals (Berényi et al. 2014; Ifft et al. 2013; Nicolelis et al. 2003; Vandecasteele et al. 2012), which is fundamental for the understanding of complex neuronal computations and higher order cognitive functions, such as learning, memory, or language (Buzsáki 2004). In addition, the reliability and performance of current invasive brain-machine interfaces, aimed to help paralyzed patients to communicate and/or interact with the outside world, significantly depend on the simultaneous recording of a high number of stable single units (Hochberg et al. 2006; Nicolelis 2003; Nicolelis and Lebedev 2009).

Currently, tetrodes and silicon polytrodes using microelectromechanical systems (MEMS) technologies are the main tools of neuroscience laboratories performing extracellular electrophysiological experiments (Berényi et al. 2014; Blanche

Address for reprint requests and other correspondence: I. Ulbert, Institute of Cognitive Neuroscience and Psychology, Research Centre for Natural Sciences, Hungarian Academy of Sciences, Magyar tudósok körútja 2, Budapest, H-1117, Hungary (e-mail: ulbert.istvan@ttk.mta.hu).

  ISSN 0022-3077.

et al. 2005; Bragin et al. 2000; Csicsvari et al. 2003; Lopez et al. 2014; Mechler et al. 2011; Nguyen et al. 2009; Seidl et al. 2012). Despite the advantage of multiple recording sites, usually these devices need to be physically moved in the brain tissue after implantation to find the desired locations of neuronal activity. The mechanical positioning of multielectrodes may damage a large amount of axons and dendrites and increases the possibility of rupturing blood vessels, which in turn can alter neuronal activity (Yip et al. 1996). Furthermore, recording from multiple brain regions (e.g., investigating the thalamocortical network) may require multiple penetrations from several recording probes, which further increases the severity of brain damage.

One possibility to limit the adverse effects of mechanical translation of multielectrodes is the concept of electronic depth control (EDC; Neves et al. 2008), which enables the electronic selection of individual recording sites from high-density, silicon-based multielectrode arrays with the aid of dedicated control software (Dombovari et al. 2014; Seidl et al. 2010, 2011, 2012; Torfs et al. 2011). The recently developed complementary metal-oxide semiconductor (CMOS)-based EDC microprobes are able to record from many brain regions simultaneously and to fine-tune independent recording positions according to the experimental needs without the physical movement of the probe.

In this study, we evaluated the in vivo performance of the two-dimensional, four-shank EDC probes by recording local field potentials (LFP) and single- and multiple-unit activity (SUA and MUA, respectively) from the thalamus and neocortex of rats and mice anesthetized with ketamine-xylazine. Particular attention has been paid to the somatosensory and auditory thalamocortical system of the animals. In rats, we quantified the amount of recorded well-isolated single units and investigated the spatiotemporal dynamics of the thalamocortical slow-wave activity (SWA) and the tonotopic organization of the auditory thalamus. In mice, optogenetic experiments were conducted to examine thalamic activity to optical stimulation of the neocortex using blue light laser pulses sufficient to evoke neuronal responses.

MATERIALS AND METHODS

Animal Surgery

Rat experiments. Wistar rats (n = 41, 150–440 g, sex balanced) were used for the acute experiments. All experiments were performed according to European Union Council Directive 86/89/EEC (November 24, 1986), and all procedures were reviewed and approved by the local ethical committee and the Hungarian Central Agricultural Office (license no. 22.1/4228/003/2009). Animals were anesthetized with a mixture of ketamine (75 mg/kg body wt) and xylazine (10 mg/kg body wt). Supplementary intramuscular ketamine-xylazine injections were given to maintain the depth of anesthesia during the recording sessions. Probes were positioned over the trunk region of the primary somatosensory cortex [S1Tr; n = 37, target: anteroposterior (AP) −2.7 mm, mediolateral (ML) 2.2 mm with respect to the bregma; coordinates measured at the tip of the first probe shaft; remaining shafts were located laterally (Paxinos and Watson 2007)] and inserted with a speed of about 1 mm/min. The tip of the probe reached a depth of ~7 mm below the dura mater, to be able to record from the hippocampus and various thalamic nuclei. The shafts of the EDC probe were oriented parallel with the coronal plane. Before insertion, the dura mater was opened to facilitate the implantation of the silicon probe and to reduce brain dimpling. In other cases (n = 4), the probe was inserted into the auditory cortex (A1; Paxinos and Watson 2007) at a 70° angle from vertical in the coronal plane to position the shafts perpendicular to the brain surface and to reach both auditory areas, the auditory cortex (AC) and the medial geniculate body (MGB), with a single penetration (see Fig. 9). The shafts of the EDC probe were oriented parallel with either the coronal [n = 3; target: AP −6 mm, dorsoventral (DV) 3.5 mm with respect to the bregma; coordinates measured at the tip of the first probe shaft; remaining shafts were located ventrally] or the sagittal plane (n = 1; target: AP −4.8 mm, DV 4 mm with respect to the bregma; coordinates measured at the tip of the first probe shaft; remaining shafts were located posteriorly). During each experiment, care was taken to avoid large blood vessels during probe implantation. Room-temperature saline solution was poured into the cavity of the craniotomy and was refilled regularly to prevent desiccation of the cortex.

Mouse experiments. Three adult Thy1-channelrhodopsin-2 (ChR2)-enhanced yellow fluorescent protein (EYFP; line 18) mice (~80 days old, 28–30 g, male) were used for the optogenetic experiments. All procedures were performed according to the ethical guidelines of the Institute of Experimental Medicine of the Hungarian Academy of Sciences and were approved by the Ethical Committee (XIV-I-001/2328-4/2012). Surgery and experiments were conducted under ketamine-xylazine anesthesia. Mice received an intraperitoneal injection of ketamine (83 mg/kg body wt) and xylazine (3.3 mg/kg body wt). The anesthesia was maintained with intramuscular injections of the narcotic (0.05 ml) every hour during the entire period of the experiments. The EDC probe was moved above the somatosensory cortex (S1; AP −1.4 mm, ML 0.5 mm with respect to the bregma; Paxinos et al. 2001) and inserted slowly (1 mm/min, driven by hand) to a depth of 5 mm. The shafts of the EDC probe were oriented parallel with the coronal plane. Before the insertion, the dura mater was removed and the exposed brain surface was covered with room-temperature saline solution to prevent desiccation of the cortex. The position of the implanted EDC probe allowed us to sample the neuronal activity of several medial, intralaminar, somatosensory, and motor thalamic nuclei of the mouse (see Fig. 11).

Electrophysiological Recordings

Electronic depth control system. The principle of electronic depth control (EDC) is the electronic selection of recording sites independently along the probe shafts of high-density microelectrode arrays. Detailed descriptions of the EDC system with the corresponding CMOS probes were published earlier (Seidl et al. 2011, 2012; Torfs et al. 2011). Briefly, the EDC system used in this study comprises four main components: four-shank CMOS probes with an integrated switching matrix, an interface box, an analog-to-digital converter, and dedicated software to control the electrode selection and data acquisition. The probes and the interface box were custom manufactured. For analog-to-digital conversion, we used either a peripheral component interconnect (PCI) multifunction data acquisition board designed for desktop computers (PCI-6259; National Instruments, Austin, TX) or a device capable of transmitting the acquired data via universal serial bus (USB) connection (USB-6353; National Instruments). The latter was also used to build a portable system that was applied in the mouse experiments. The software component of the system is described in *Software control*.

The EDC probe has four 8-mm-long needle-like shafts (thickness: 50 μm, width: 160 μm; Fig. 1*A*). The shafts of the probe are placed 550 μm apart, with each shaft comprising 257 iridium oxide (IrO_x) recording sites with a diameter of 50 μm. The recording sites are arranged in two columns and are covering the complete probe shaft, comprising 254 equally spaced round electrodes with a horizontal and vertical pitch of 60 μm (Fig. 1*A*, *bottom*). Three additional recording sites, one with a triangular shape and two circular electrodes, are implemented in the tip region of the probe. The average impedance of

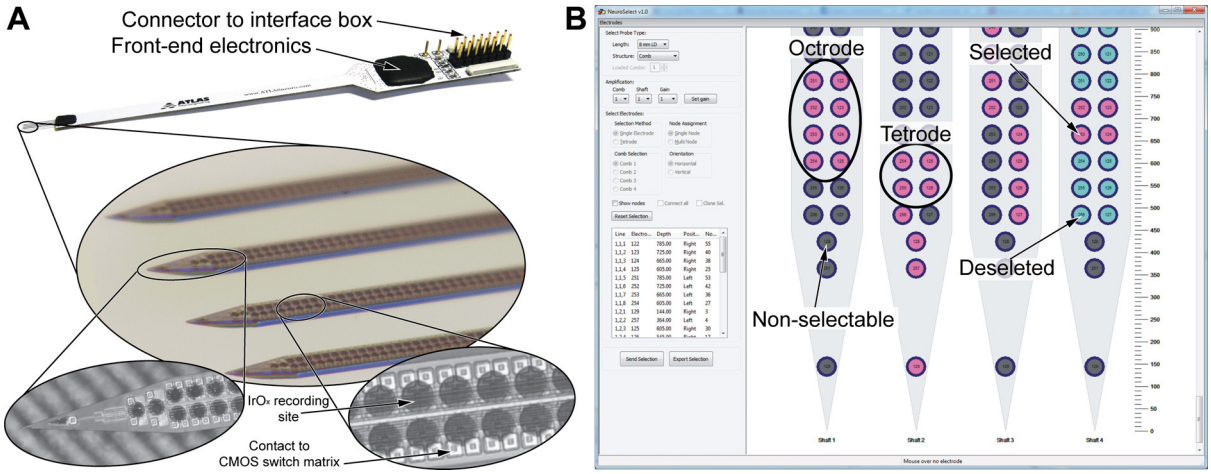

Fig. 1. The 4-shaft, 1,028-site electronic depth control (EDC) probe and the graphical user interface of the NeuroSelect software used to control the electrode selection. *A*: the probe design for acute recordings comprises the 4-shaft silicon comblike probe connected to a printed circuit board, the front-end electronics, and the connector to the interface box (*top*). Each of the 8-mm-long shafts (*middle*) comprises 257 IrO_x recording sites evenly distributed in 2 columns along the entire shaft length with an electrode pitch (center to center) of 60 μm (*bottom right*; only a small section of the shaft is shown). All electrodes have a circular shape except for the triangular-shaped electrode located at the tip of the probe (*bottom left*). The CMOS-based switching electronics are located underneath the recording sites. Note that the probe shown has a pointy tip, whereas probes used in acute experiments had a chisel-shaped tip. *B*: electrode selection panel of the dedicated control software (NeuroSelect) used to address the user-defined recording sites. Several probe types with different shaft lengths can be selected from a predefined list (*top left*). Eight individual recording sites can be selected on each shaft. Selected, deselected, or nonselectable electrodes are color coded. The tetrode selection method and the clone selection option can accelerate the process of electrode selection (*middle left*). The selection of tetrodes or octrodes is recommended for single-unit activity recordings and subsequent spike sorting.

the recording sites was 300 ± 175 kΩ (Torfs et al. 2011). The electronic components of the EDC design integrated on the probe shaft (e.g., connection matrix, switching electronics, control, input and output lines) were realized using a commercial 0.5-μm-CMOS process (Torfs et al. 2011). Successive post-CMOS microfabrication steps, as detailed in Seidl et al. (2011), were accomplished to define probe shape and the deposition of the IrO_x electrodes as well as the corresponding recording site metallization at the base of the silicon probe. The connection matrix and the switching electronics of the EDC probes are used to connect every recording site to the analog output lines ($n = 8$ per shaft, 4 shafts $\times$ 8 = 32 output lines in total). Each recording site can be electrically connected to four of the eight output lines. The input and output lines of the probe designed for acute in vivo recordings are wire bonded to a printed circuit board (PCB) and sealed with technical grade epoxy resin. In addition, chronic probes with flexible polyimide cables were also manufactured (Seidl et al. 2011). Before insertion, probes were first soaked for at least 30 min in a 1% solution of an anionic detergent containing protease enzymes (Terg-a-zyme; Alconox, White Plains, NY) and then rinsed thoroughly in distilled water. The same procedure was repeated to clean the probes after explantation. Probes were reused multiple times in consecutive acute recordings without significant decrease in their recording performance. A total of four probes with a chisel-shaped tip were used during all experiments ($n = 41$ rat and $n = 3$ mice experiments). Two stainless steel needles inserted in the nuchal muscles of the animal served as the reference and ground electrodes during the recordings. The recorded signals were preamplified (gain: 37 dB), filtered (bandpass filter: 0.1–8,500 Hz), and multiplexed (8:1, with 25K samples/s per channel rate) with the aid of the front-end CMOS chip on the PCB (Fig. 1*A*, *top*), and then transmitted to the interface box.

The interface box was connected to the acute probe with a tether, transmitting the control signal, power supply, and the four analog, multiplexed recording signals. In total, the interface box can amplify and transmit the data of 128 analog output channels (i.e., the signals from 4 probes with 4 $\times$ 4 shafts). The role of the interface box is to control the probes, provide second-stage amplification (10–40 dB), and demultiplex the analog signals. High-density D-sub connectors (2 $\times$ SHC68-68-EPM; National Instruments) were used to connect the interface box to the data acquisition system. The reconstructed analog data was digitized at a sampling rate of 20 kHz/channel on 32 channels with 16-bit precision. A PCI-6259 card (National Instruments) was used in experiments performed on rats and a USB-6353 device (National Instruments) in recordings from mice. The digital data were stored on the hard drive of a personal computer or a laptop for offline analysis.

Software control. The control of the interface box and the probe can be achieved either through the data acquisition device (via the D-sub connectors) or through a separate USB connection. A dedicated software with a graphical user interface called NeuroSelect (Seidl et al. 2010) was developed using the free multiplatform wxWidgets framework and DialogBlocks, based on C++ and running under the Microsoft Windows operating system. The software allows us to select the required recording sites manually on each shaft according to the experimental situation (Fig. 1*B*). Furthermore, a "semiautomatic electrode selection mode" helps the user to select electrodes with high signal-to-noise ratio (Seidl et al. 2010) in a period of time of about 30 min for a four-shank probe; a fully automated electrode selection mode is under development, taking into account recording sites with lower signal-to-noise ratio but recording smaller amplitude units (Van Dijck et al. 2012). The experimenter can select up to eight electrodes simultaneously per shaft (see also probe description) by clicking on the small circles symbolizing the recording sites. The user can choose between different probe types (having lengths of 2, 4, and 8 mm) and probe configurations (single shaft probe, comb-like configuration with 4 shafts, 4 probes with 4 $\times$ 4 shafts). The selected, deselected, and nonselectable electrodes are color coded (Fig. 1*B*). The experimenter has the option to choose between single electrodes or tetrodes (i.e., 2 $\times$ 2 adjacent electrodes). Tetrode selection can accelerate the electrode selection process, and this type of selection is also advised during the recording of single-unit activity, to take advantage of signal triangulation. Neighboring channels can record the action potentials of the same neuron, which facilitates the separation of single units during spike sorting (Gray et al. 1995; Harris et al. 2000). Each electrode can be connected only to a limited number of output lines. This constraint of the system limits the possible electrode configurations; that is, recording sites cannot be selected in every possible arrangement. However, these forbidden configurations are small in number com-

pared with the number of valid states. Those electrodes, which cannot be programmed because of these restrictions, are disabled for user selection and are color coded in gray (Fig. 1*B*). The selected configurations can be saved in comma-separated values (CSV) files for later use. The recording sites can be configured at any time, even during data acquisition. The settling time after the electrodes are reconfigured depends on the DC mismatch between the switched electrodes and the time constant of the amplifier (Dombovari et al. 2014). Usually, it requires only a few seconds (after electrode switching) for the recorded signals to stabilize. The switching transient itself lasts about 100 ms.

The NeuroSelect software is also able to control data acquisition; i.e., it can process, display, and store the recorded signals. However, during our experiments, data acquisition and visualization of the recorded signals were performed using custom-made LabVIEW-based software (applied in our laboratory for electrophysiological recordings on a daily basis). The two software programs can run simultaneously on one computer or can be operated independently on separate computers. In our experiments we recorded 5- to 20-min-long traces and stored them as separate files. The acute recording sessions lasted 3–8 h, depending on the experimental design.

Histology

Rat experiments. After the recording session, the EDC probe was withdrawn and the animal was deeply anesthetized and perfused through the heart with saline solution followed by 4% paraformaldehyde in 0.1 M phosphate buffer (PB). The brain was removed from the skull and postfixed overnight at 4°C. The fixed brain was sectioned using a vibratome (Leica VT1200; Leica Microsystems, Wetzlar, Germany) into 60-μm-thick coronal or sagittal sections. Following washing in 0.1 M PB, sections were mounted from gelatin, air-dried, processed for cresyl violet (Nissl) staining, dehydrated in xylene (twice for 10 min), and coverslipped with DePex (SERVA Electrophoresis, Heidelberg, Germany). The sections were photographed under an AxioPlan 2 microscope (Zeiss, Jena, Germany) equipped with a DP70 digital camera (Olympus, Tokyo, Japan) to examine the tracks of the EDC probe and to verify the recording position based on the Paxinos brain atlas (Paxinos and Watson 2007). In one experiment, the backside of the probe shafts was painted with red fluorescent dye 1,1-dioctadecyl-3,3,3,3-tetramethylindocarbocyanine perchlorate (DiI; D-282, ~10% in ethanol; Life Technologies, Carlsbad, CA) to accurately determine the position of the tip of the probe (i.e., the depth of the implantation) in the brain tissue (DiCarlo et al. 1996). In this case the histological procedure was similar as described before, except that the gelatin-mounted and air-dried sections were examined under the microscope with Attoarc fluorescence illuminators using filters for Cy3 (exciting filter bandpass 530–560 nm) before Nissl staining.

Mouse experiments. After the recording session, the EDC probe was withdrawn and the animal was deeply anesthetized and perfused through the heart with saline solution followed by a fixative containing 4% paraformaldehyde and 0.1% glutaraldehyde in 0.1 M PB. The brain was removed from the skull and sectioned using a vibratome (Leica) into 100-μm-thick coronal sections. Following washing in 0.1 M PB, sections were mounted, air-dried, and coverslipped with Vectashield (Vector Laboratories, Burlingame, CA) for fluorescent microscopic observations. The sections were photographed using a microscope (Axio Scope; Zeiss) equipped with a digital camera (DP 70; Olympus) to examine the EDC probe tracks together with the EYFP signal and to verify the recording positions based on the mouse brain atlas (Paxinos et al. 2001). Brightness and contrast were adjusted, if necessary, using Adobe Photoshop 7.0 (Adobe, San Jose, CA).

Somatosensory Stimulation

Cutaneous receptive fields in the neocortex and in the thalamus were identified by listening to the recorded signal in the multiunit band (500-5,000 Hz) through a pair of loudspeakers while using a cotton bud to systematically tap the extremities, trunk, jaw, and whiskers of the animal (both rats and mice) gently, to find the areas responding to somatic stimulation. A home-built stimulator was used for stimulation in rats. A short and thin wooden stick applied to a stepper motor repetitively touched the skin of the animal at a user-defined frequency. The frequency of the stimulator could be adjusted externally through custom-made LabVIEW software (National Instruments). Stimulation frequency was usually set to ~1.5 Hz, based on the peak frequency of ketamine/xylazine-induced slow wave activity. The delivery times of the stimuli were recorded on a separate trigger channel. After the experiments were completed, the recorded evoked MUA responses were averaged. These MUA averages were used to facilitate the determination of the approximate position of the borders between adjacent thalamic nuclei and to support the histology-based localization of the probe's position in the brain (see Fig. 7*C*).

Auditory Stimulation in Rats

After the surgery, the skull of the animal was fixed to the stereotaxic frame with a custom-made metal holder. One part of the holder was attached to the stereotaxic frame with two screws, and the other part was glued to the cleaned, frontal part of the skull of the rat. With the application of the holder, we could improve the fixation of the head and remove the ear bar from the right ear (contralateral to the craniotomy) without accidentally moving or relocating the skull. The holder reliably stabilized the animal's head during the entire duration of the experiment; thus the probability of damaging the silicon probe due to sudden changes of the head position, attributable to the modified setup, was very low. After the removal of the ear bar, a loudspeaker (KFC-T201; Kenwood, Tokyo, Japan) was placed 2 cm away from the right ear of the rat. Acoustic stimuli were generated using a personal computer-controlled sound generator [RP2 Real-Time Processor; Tucker-Davis Technologies (TDT), Alachua, FL] and amplified with a headphone buffer (HB7; TDT). Three types of acoustic stimuli were delivered during the experiments: click trains (rectangular pulses, duration: 0.1 ms), wideband Gaussian noise pulses (duration: 100 ms), or pure tone pips (duration: 100 ms). The latter were covering a wide range of the auditory spectrum of rats (12 different frequencies ranging from 4 to 20 kHz). Intensities and repetition rates of the stimuli were adjusted based on the design of the actual experiment (intensity range: 30–90 dB SPL, range of repetition rate: 0.7–3 s^{-1}). Three hundred trials were obtained for click pulses and Gaussian noise, and 20 trials for the pure tones. The delivery times of acoustic stimuli were recorded on a separate trigger channel.

Optogenetic Stimulation in Mice

Photoactivation of the somatosensory cortex was achieved by 5-ms-long blue laser light pulses delivered to the surface of the cortex. The bone of the skull over the frontal and somatosensory cortices was thinned down to ~0.1 mm. The surface was moistened with saline to keep this thin layer of bone transparent. The optic fiber was placed immediately above the bone to activate the ChR2-positive layer 5 pyramidal cells. The following custom optical system was used for fiber optic light delivery: the beam generated by a 473-nm DPSS laser (LRS-0473-PFM-00100-03; Laserglow Technologies, Toronto, ON, Canada) was used via a fiberport (Thorlabs, Newton, NJ) and a fiber optic patchcord (105 μm, 0.22 NA; Thorlabs) to the optic fiber (100-μm diameter). The maximum power density measured at the output of the delivery fiber was 17 mW (1,360 mW/mm^2). Light intensity was modulated with the adjust knob on the DPSS power supply. Stimulus trains of 10 pulses were given at 1 or 20 Hz, with

0.8-mW (97 mW/mm^2) stimulus intensity. The trigger TTL pulse for the light pulse trains was generated by a Master-8 stimulator (A.M.P.I., Jerusalem, Israel). The first recording channel was used as a trigger channel to record the delivery times of the laser stimuli.

Data Analysis

The raw data were analyzed with Neuroscan 4.3 software (Compumedics, El Paso, TX) and using scripts written in MATLAB (The MathWorks, Natick, MA). Spike sorting was performed in Linux (Ubuntu 10.04 LTS) with custom-written scripts and with dedicated software (Klusters) used for clustering of single units (Hazan et al. 2006).

Calculation of the signal-to-noise ratio. The signal-to-noise ratio (SNR) of cortical and thalamic recordings was calculated using the MATLAB implementation of the adaptive-threshold spike detection method (STH) described in Seidl et al. (2010). First, the wideband data was bandpass filtered (500-5,000 Hz, zero phase shift, 24 dB/octave) to obtain the unit activity. After that, we applied the STH method on the filtered traces. A 30-s-long section of the recordings was used to compute the SNR. Traces containing large artifacts or high-frequency noise contaminating the unit activity were excluded from the analysis. However, because of the large amount of investigated recordings, we included traces recorded with electrodes located in areas without neurons (ventricles, white matter, brain surface) and showed SNR values close to zero.

Spike sorting. Spike sorting was performed individually on each shaft. Electrodes were selected in groups of octrodes (8 recording sites next to each other) to improve the unit isolation. The continuous, wideband signals were digitally bandpass filtered (500-5,000 Hz, zero phase shift, 24 dB/octave) to remove local field potentials. Spikes with a power of greater than five times the standard deviation of the root mean square (RMS) of the filtered traces were detected and extracted (Csicsvari et al. 1998). The threshold level was calculated automatically. The extracted spike waveforms were aligned to their negative peaks, and the first three principal components (PCs) were calculated for each of the detected action potentials on each of the channels. Therefore, a single spike was represented as a 24-dimensional feature vector (8 channels $\times$ 3 PCs). Units were identified and isolated manually with cluster-cutting software (Klusters; Hazan et al. 2006). Autocorrelograms were checked for clear refractory periods (no spikes in the range of $<$3 ms), which was one of the criteria for good unit isolation. Another criterion was that the points of the separated neuron cluster were clearly isolated from the rest of the points in at least one of the planes of the waveform parameters. Figure 5*A* shows the end result of spike sorting of a representative recording with four well-separated clusters. The width of mean action potential waveforms was calculated to differentiate between principal cells and interneurons (Bartho et al. 2004). The spike width was defined as either the time difference between the two positive peaks of the spike (P1-P2 width) or as the time difference between the two points of the spike crossing the zero voltage level (zero-crossing width).

Protocol for mapping thalamocortical activity. To facilitate the investigation of the spatial and temporal properties of the thalamocortical slow-wave activity, recording sites of the EDC probe were selected in the following way. Two adjacent electrodes recording good quality cortical MUA (located usually in layer 5 of the cortex) were selected on each shaft, whereas the remaining six recording sites were positioned in the thalamus side by side (see Fig. 6*A*, *1*). With this configuration, we were able to record the ongoing thalamocortical oscillations simultaneously from eight relatively independent brain positions: four thalamic and four cortical locations (minimal distance of $\sim$500 μm between the locations). The thalamic electrodes located at the tip of the probe were selected before the first recording. After 5- to 10-min-long intervals of data acquisition, the actual group of thalamic recording sites was reset, and the 6 nonoverlapping nearest sites located dorsally to the previous set were selected (see Fig. 6*A*, *2*). The position of electrodes selected for recording cortical activity was not changed during the whole mapping process. The thalamic "record-reselect-record" steps described above were repeated until the top of the thalamus was reached (see Fig. 6*A*, *N*), which was indicated by the lack of thalamic MUA and the appearance of hippocampal gamma oscillations. Usually, 10–11 steps were necessary to map the thalamus covered by the probe.

Detection of slow-wave activity states. We detected the different states of slow-wave activity (SWA) as described in our previous article (Fiáth et al. 2016; "up-states" with high unit activity and "down-states" with low unit activity; see Figs. 2 and 6*B*). Briefly, we filtered the wideband data to obtain the MUA signal (bandpass filter 500-5,000 Hz, zero phase shift, 24 dB/octave, rectification; see Fig. 6*B*, *1*). Next, it was downsampled from 20 kHz to 2 kHz, and then the envelope of the downsampled MUA was extracted with an additional low-pass filter (zero phase shift, 30 Hz, 24 dB/octave; see Fig. 6*B*, *2*). The envelope signal served to establish up- and down-state onsets. The average amplitude (AVG) and standard deviation (SD) of the MUA during down-states was calculated. These values were used to determine a threshold level to find the up- and down-state onsets in the cortex and in the thalamus (see Fig. 6*B*, Th_{Ctx} and Th_{Thal}, respectively). The threshold was empirically set to AVG + (3 SD), which resulted in an accurate detection of state onsets (see Fig. 6*B*, *3*). Traces containing large artifacts or high-frequency noise contaminating the unit activity were excluded from the analysis.

Based on our empirical observations and on data found in the literature (Mukovski et al. 2007; Sakata and Harris 2009; Saleem et al. 2010), the minimum duration of up-states was set to 50 ms, whereas the minimum duration of down-states was chosen to be 100 ms. The onset of an up (down)-state was defined as the time point at which the value of the MUA envelope exceeded (fell below) the calculated threshold level. This time point had to be preceded by an opposite state with a duration equal to or longer than the defined minimal state duration. Finally, the calculated onset times of up- and down-states were saved in separate files for every cortical and thalamic channel.

Calculation of the up-state onset time difference color map. After extracting cortical and thalamic up-state onsets, we aimed to investigate the temporal variability in the initiation of cortical vs. thalamic up-states. On each shaft, the two cortical electrodes recorded the unit activity virtually from the same location, because these sites were selected adjacent to each other. To remove the resulting redundancy, only the cortical channel with the higher up-state/down-state MUA ratio was chosen on each shaft for further analysis. To determine the time difference between the onset of cortical and thalamic up-states, the time value corresponding to a cortical up-state onset was subtracted from the time value of a thalamic up-state onset (see Fig. 6*B*, *4*). As a result, a positive value indicates that the cortical up-state started before the thalamic up-state, whereas a negative value means that the cortical up-state was preceded by the thalamic up-state. For each cortical up-state, the up-state onset time differences were calculated between the up-states detected on all thalamic traces (24 channels) in a time window of $-$300 to 300 ms around the given cortical up-state. Between each cortical and thalamic channel, a histogram was created from the calculated up-state onset time difference values (see Fig. 7*E* for examples). Finally, to visualize the variability of up-state initiation between cortex and thalamus in a comprehensible way, the average and standard deviation of the time difference values were calculated and two-dimensional color maps were constructed from the derived data set (see Fig. 7*B*). In the case of four cortical locations (one found on each shaft), the analysis resulted in eight color maps, two for each shaft.

Construction of tonotopic color maps. To determine tonotopy in rats, 12 different pure tone pips between 4 and 20 kHz were presented to the animal (duration: 100 ms, intensity: 70 dB, onset/offset time: 5 ms, repetition rate: 1 s^{-1}). To prepare simple tonotopic maps for cortical and thalamic areas, a tetrode (4 adjacent recording sites) with the best sound-evoked MUA response was selected in the auditory

cortex on each shaft, and another tetrode was selected in the thalamus (starting at the tip of the shafts). After the presentation of all 12 clear tone frequencies ($n = 20$ stimuli for each frequency delivered in quasi-random order), with the simultaneous recording of the wideband electrical activity from the selected locations, the thalamic tetrode was shifted to new, adjacent, and nonoverlapping positions. The cortical tetrode position was not moved during the whole mapping procedure. These steps were repeated as long as sound-evoked responses could be recorded from the thalamus or the hippocampus was reached. In total, 10 different tetrode positions were selected in the thalamus during the experimental session, which corresponds to a vertical coverage of ~1.1 mm. To extract population activity, wideband recordings were first bandpass filtered (between 500 and 5,000 Hz, zero phase shift, 24 dB/octave). The integral of the first 100-ms-long section of mean sound-evoked MUA responses (starting from the onset of the sound stimulus) and the peak amplitude during the same time interval were computed and illustrated on separate color maps (see Fig. 10, *A* and B).

Data analysis of optogenetic mouse experiments. To map the thalamic MUA responses elicited by optical stimulation, we used a protocol similar to that used during the rat experiments described above. Octrodes were selected in the thalamus on each shaft, starting at the tip of the EDC probe. Next, we recorded the wideband thalamic activity while simultaneously stimulating the somatosensory cortex with blue laser light pulses. After the optical stimulation protocol was finished, new octrodes were selected above the former ones (i.e., at a more dorsal position). The optical stimulation protocol was repeated while the thalamic responses were recorded from the new positions. This procedure was carried on until the top of the thalamus was reached.

To calculate optically evoked thalamic MUA responses, the wideband data were filtered in the multiunit band (see above). From the continuous MUA traces, 150-ms-long trials containing the evoked responses were extracted. These trials were then averaged within each channel to compute the average MUA response to optical stimulation at every thalamic position. After that, the peak amplitude corresponding to each average MUA response was detected with a custom-written MATLAB script. Using the obtained peak values, we constructed color maps for both stimulation frequencies (see Fig. 11, *D* and *E*).

The spike-sorting procedure used to extract single units from the mouse data was the same as that described above. Last, peristimulus time histograms (PSTH) with 1-ms bin width were created from the spikes of the sorted single units and the delivery times of laser pulses (see Fig. 11*G*).

RESULTS

Electrophysiological Recording Capabilities of the EDC System

The EDC system was validated in acute experiments in rats and mice anesthetized with ketamine-xylazine. One aim of the experiments was to exploit the advantages of the novel recording system, that is, to record LFP and unit activity from multiple distinct brain regions simultaneously and to obtain the activity of numerous single units with high separation quality. The application of ketamine-xylazine is known to induce a characteristic brain rhythm called slow-wave activity (SWA; Steriade et al. 1993a, 1993b, 1993c). The ketamine-xylazine-induced SWA shares many features with slow waves emerging during natural slow-wave sleep (Crunelli and Hughes 2010; Steriade et al. 1993c); therefore, it is used as a general model of the physiological SWA (Crunelli and Hughes 2010). Both the physiological SWA and the SWA induced by ketamine-xylazine has a dominant spectral peak in the 0.5- to 2-Hz frequency range and is composed of two alternating states, the up-state with high synaptic activity and action potential firing and the down-state with a significantly decreased neuronal activity. SWA can be recorded from the entire neocortex (Fig. 2*A*) and from most parts of the thalamus (Fig. 2*B*). The innovative features of the EDC system (electronic selection of recording sites in distinct brain regions without the need of mechanical probe translation, and individual and dynamic fine-tuning of recording locations) allow the simultaneous investigation of the activity on multiple individual thalamic and cortical sites to assess the neuronal mechanisms underlying SWA and also other, faster brain oscillations (e.g., sleep spindle, gamma) grouped by this particular rhythm (Clemens et al. 2007; Molle et al. 2002).

Depending on the experimental needs, a variety of recording site configurations can be used with the EDC system. For example, if our focus is on single-unit activity (SUA), the electronic selection of adjacent recording sites (e.g., 4 sites, called tetrodes, or 8 sites, called octrodes) will be more effective (Figs. 2*A* and 5) compared with configurations using nonadjacent electrodes (Fig. 2*B*). Recording the spikes of the same neuron on multiple, closely located electrodes significantly enhances the quality of spike sorting and increases the single-unit yield (Gray et al. 1995; Harris et al. 2000; Quiroga 2012; Rey et al. 2015). On the other hand, with a different configuration, where the recording sites are selected apart from each other with equal spacing (Fig. 2*B*), it is possible to investigate the dynamics of the neuronal activity inside a larger structure or on a global scale, between distinct brain areas. Furthermore, the large vertical coverage of the probe (8 mm/shaft) and the combination of local (tetrodes or octrodes) and global (single electrodes distributed equally or unequally on the shafts) electrode configurations enable the simultaneous examination of the relationship between LFP and unit activity (MUA or SUA) in multiple brain regions.

To demonstrate the electrophysiological performance of the EDC probe, first we calculated the signal-to-noise ratio (SNR) of cortical and thalamic MUA traces (Fig. 3). The data of several thousand recording sites of several experiments were examined (thalamus: ~8,000 electrodes, cortex: ~5,000 electrodes). The average SNR was 2.48 ± 2.68 in the cortex (Fig. 3, *A* and *C*) and 4.13 ± 2.47 in the thalamus (Fig. 3, *B* and *D*). Recording sites with zero or very low SNR values were located either in areas without neurons (ventricles, white matter, brain surface) or in the supragranular layers of the neocortex (see Fig. 3, *A* and *B*). However, the significant number of high SNR values is in agreement with the fact that high-quality SUA could be recorded with the EDC probe during most of the experiments. Furthermore, SNR values above 4 suggest the presence of clearly separable SUA (Kim et al. 2010).

In the case of electrophysiological experiments, it is crucial to know the exact location of recording sites in the brain tissue. Using fluorescent stains (e.g., DiI), we can reconstruct the probe tracks in fixed brain sections and correlate the physiological recordings with the underlying anatomy (Fig. 4*A*). Because the position of the probe tip is determined by the implantation depth, preparing Nissl-stained sections is adequate to find the tracks made by the probe's four shafts and to estimate the recording positions (see Figs. 4*B*, 5*C*, 7*B*, 9*A*, and 11*C*). However, for a more accurate estimation of the position

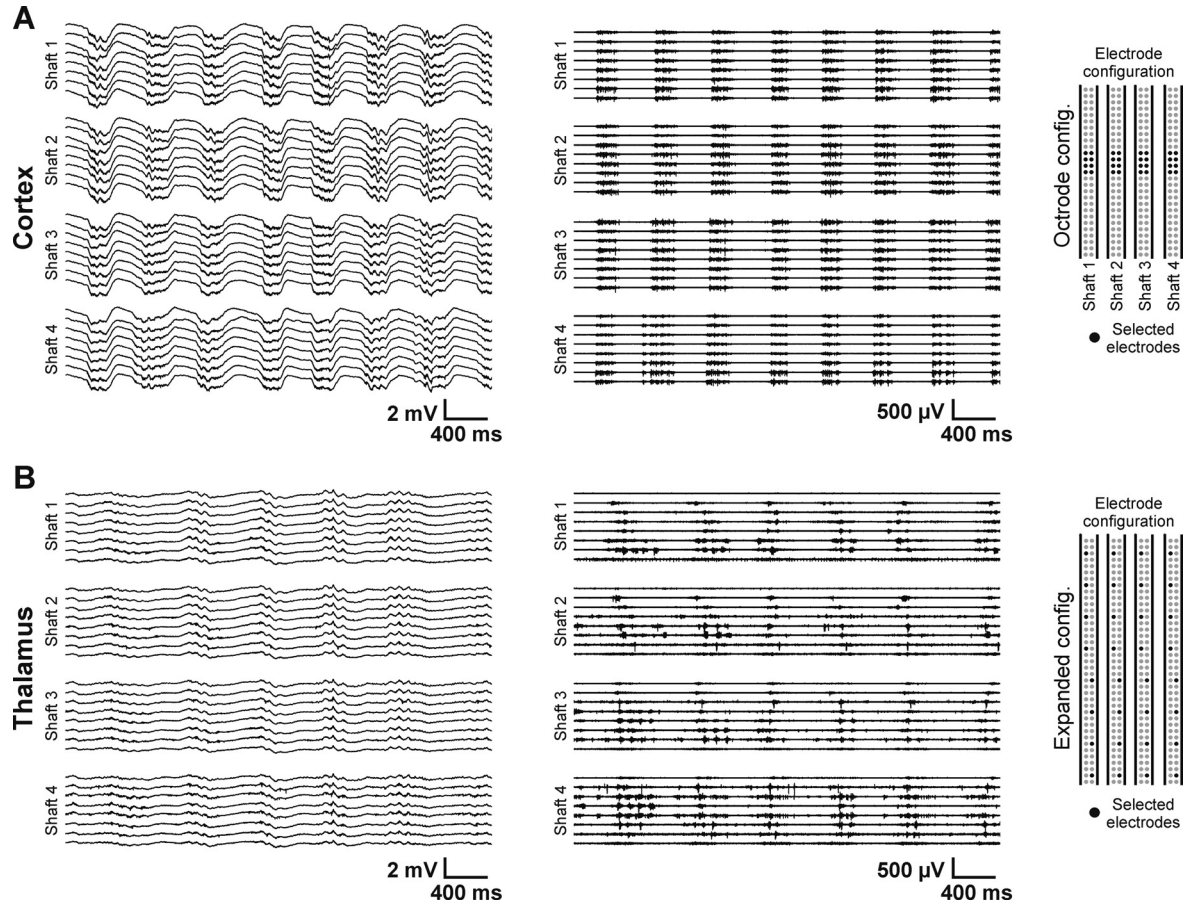

Fig. 2. Representative 4-s-long continuous traces recorded with the 4-shank EDC probe. *A*: wideband recording (*left*; 0.1–8,500 Hz) and unit activity (*middle*; obtained by filtering the trace at *left* between 500 and 5,000 Hz) from layer 5 of the somatosensory cortex of the rat under ketamine-xylazine anesthesia. On each shaft, 8 adjacent recording sites were selected (octrode configuration; *right*). The rhythmic alternation of anesthesia-induced slow waves can be observed on the traces, with high unit activity during up-states and the absence of spikes during down-states. Note the quasi-synchronous onset of up-states between the cortical channels. *B*: wideband (*left*) and unit activity (*middle*) recordings from the thalamus of another anesthetized rat. In this case, the selected recording sites were distributed with equal distances along the probe shafts covering a vertical distance of ~2 mm (expanded configuration; *right*). The electrodes recorded the activity of several thalamic nuclei and regions adjacent to the thalamus. The slow-wave activity is present in the thalamus, as well, but the spatiotemporal properties of thalamic slow waves are different compared with the cortex.

of individual recording sites, more selective staining procedures are recommended or the application of sensory, electrical, or optical stimulation (e.g., somatosensory stimulation, see Fig. 7*C*).

SUA Recorded with the EDC Probe

To assess the single-unit recording capabilities of the EDC probes, we implanted them into neocortical and thalamic areas of ketamine-xylazine-anesthetized rats and recorded the SUA with octrode configuration (Fig. 2*A*). Spike sorting was performed on the recorded data offline using manual cluster cutting (Fig. 5*A*). Because the extracellular action potential amplitudes decrease rapidly as a function of distance from the neuron (Buzsáki 2004; Henze et al. 2000), and because the intershaft distance of the EDC probe is 550 μm, electrodes located on adjacent shafts cannot record spikes originating from the same neuron. Therefore, we did the spike sorting separately on each shaft. It may also happen that the action potentials of a neuron are detected on recording sites of adjacent but nonoverlapping octrodes located on the same shaft. In this case, if the spike amplitudes are sufficiently large on both recording sites, the spikes of this particular neuron will be isolated two times. However, the relatively large size of the electrodes and the rapid spatial decrease of spike amplitudes keeps the amount of redundant units minimal (<5%). We did not attempt to exclude redundant units for now; therefore, a few of them might be included in the analysis.

In total, n = 1,837 units were isolated from 28 rats. Well-separated neurons were mostly found in the thalamus (average: 55.2 ± 16.53 per experiment, range: 27–91), while unit yields in the cortex were usually lower (average: 32.64 ± 22.63 per experiment, range: 9–85). The mean peak-to-peak amplitude of recorded thalamic units was 119.83 ± 58.24 μV (maximum: 444.7 μV), whereas the average spike amplitude in the cortex was 61.83 ± 33.4 μV (maximum: 240.35 μV). The average number of neurons that could be detected simultaneously with a single octrode was 1.16 ± 0.4 (range: 0–8) in the thalamus and 0.6 ± 0.3 (range: 0–6) in the cortex. In our opinion, the putative reasons behind the lower cortical unit yield are the sparse firing of neurons located in the supragranular cortical layers (de Kock et al. 2007; de Kock and Sakmann 2009; Petersen and Crochet 2013; Sakata and Harris 2009) and the smaller dorsoventral extension of the cortex compared with the thalamus, but we cannot exclude the possibility that the im-

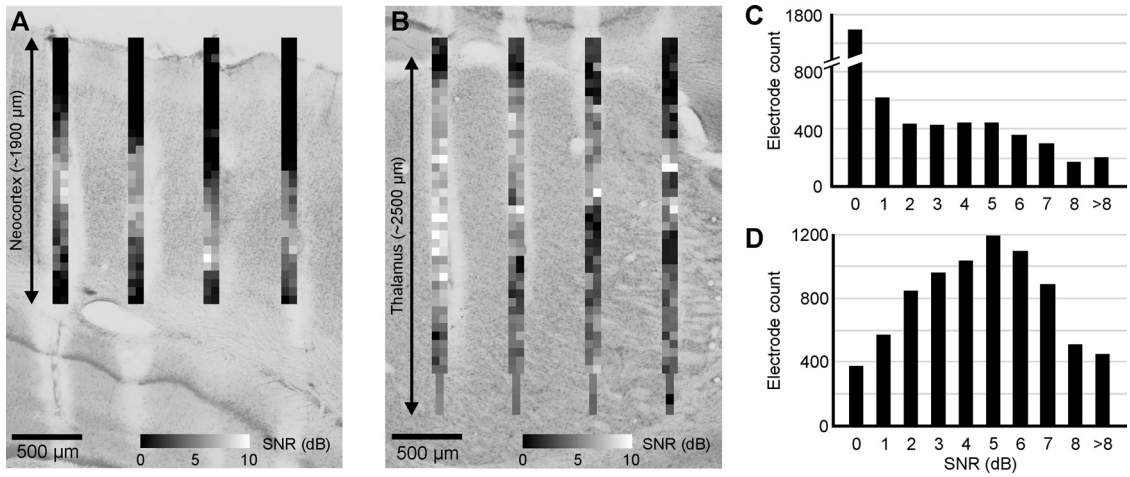

Fig. 3. Signal-to-noise ratio (SNR) of cortical and thalamic unit activity recorded with the EDC probe. *A*: 2-dimensional SNR map calculated from the cortical recordings of a representative experiment. Each SNR value corresponds to a single recording site. The Nissl-stained coronal section in the background shows the corresponding cortical area with the tracks of the probe. Note that the highest SNR values are located in the granular and infragranular layers of the cortex. *B*: SNR map calculated in the thalamus of the same animal as in *A* with the corresponding thalamic anatomy. *C*: distribution of all calculated cortical SNR values. *D*: distribution of all calculated thalamic SNR values.

plantation of the silicon probe might cause slightly larger damage to the cortical than to thalamic tissue.

The action potential waveform of single units clearly appeared on multiple recording sites (Fig. 5*A*, *bottom, left* and *right*; Fig. 5*D*). Most of the thalamic neurons fired in burst mode under ketamine-xylazine anesthesia, as shown by peaks on their autocorrelograms (Fig. 5, *A* and *B*). After histological processing, the brain position of the recorded single units was estimated on the basis of Nissl-stained sections containing the probe tracks (Fig. 5*C*). Furthermore, physiological and firing properties (e.g., intraburst spike count) of the recorded neurons could help to classify them into different groups. The spatiotemporal distribution of the recorded potential field depends on the type and morphology of the recorded cell (Blanche et al. 2005; Delgado Ruz and Schultz 2014). Therefore, the two-dimensional distribution of extracellular action potential waveforms could be used to discriminate between putative pyramidal cells, thalamocortical neurons, or interneurons (Fig. 5*D*). Furthermore, several properties of the spike waveform, such as the spike width, are good candidates to identify putative excitatory (wide spikes; Fig. 5*E*) or inhibitory cells (narrow spikes; Bartho et al. 2004; Fig. 5*E*). Also, we recorded action potentials from the internal capsule, a white matter structure containing axonal fibers. These putative axonal spikes had short durations (Fig. 5*E*) and a triphasic characteristic, which is in agreement with the results obtained by Robbins et al. (2013).

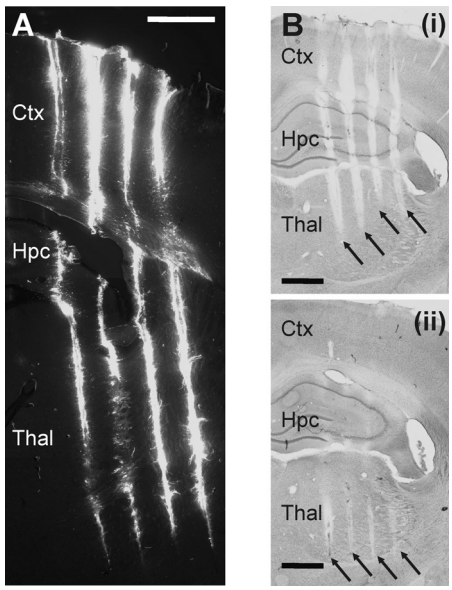

Fig. 4. Postmortem histological reconstruction of the probe tracks to determine the location of the EDC probe in the rat brain. *A*: fluorescent micrograph of a coronal rat brain section containing the tracks of the 4 shafts of the EDC probe. The back side of the shafts was painted with DiI before the acute experiment. The tip of the shafts can be clearly located. Scale bar, 1 mm. *B*: light microscopic image of two 60-μm-thick Nissl-stained coronal rat brain sections showing the 4 tracks of the probe. The 2 sections displayed are not adjacent; there was an additional section located between them (not shown). Black arrows point to the tracks made by different shafts. The reason for the visibility of the tracks on multiple sections is presumably due to the oblique cutting of the fixed brain before staining. Scale bar, 1 mm. Based on the tracks visible on Nissl-stained sections and the known penetration depth, the approximate position of recording sites can be determined, together with the main structures from which the neuronal activity was recorded. Ctx, neocortex; Hpc, hippocampus; Thal, thalamus.

Spatiotemporal Dynamics of the Thalamocortical SWA

One of the mentioned advantages of the EDC probe is that we can record from multiple brain regions simultaneously without the need to insert additional recording electrodes into the brain tissue or move the implanted probe to new positions. Recording sites with the best signal quality can be selected electronically and can be reselected any time to record from another brain position. This is particularly advantageous for the investigation of brain functions, which are generated in widespread neuronal networks. The SWA described above originates in the thalamocortical network (Steriade et al. 1993a, 1993c, 2001). The primary generator of this particular brain rhythm is the neocortex; however, growing scientific evidence suggests an important role of the thalamus in the shaping and maintenance of SWA (Crunelli et al. 2015; Crunelli and Hughes 2010; David et al. 2013; Gemignani et al. 2012; Lemieux et al. 2014). Therefore, the simultaneous examination

of these two structures is inevitable for the deeper understanding of the mechanism underlying SWA.

There is only a limited number of studies investigating the dynamics of the SWA in the thalamocortical network, partially due to the complexity of these experiments, that is, the need for numerous recording sites placed in multiple areas of the neocortex and thalamus (Sheroziya and Timofeev 2014). However, the EDC system is well-suited to simultaneously sample the electrical activity in a high number of distinct thalamic and cortical areas. To investigate the spatiotemporal dynamics of the SWA, we first recorded the wideband activity from the thalamocortical network of ketamine-xylazine-anesthetized rats with a predefined protocol and obtained the MUA-based onset time for each up-state (see MATERIALS AND METHODS for details; Fig. 6, *A* and *B*). In the next step, we calculated the time difference between the onset of the detected cortical and thalamic up-states (Fig. 6*B4*) and depicted the mean and standard deviation of the time difference values in the form of two-dimensional color maps (Fig. 7, *A* and *B*). Mechanical somatosensory stimulation was used to facilitate the histology-

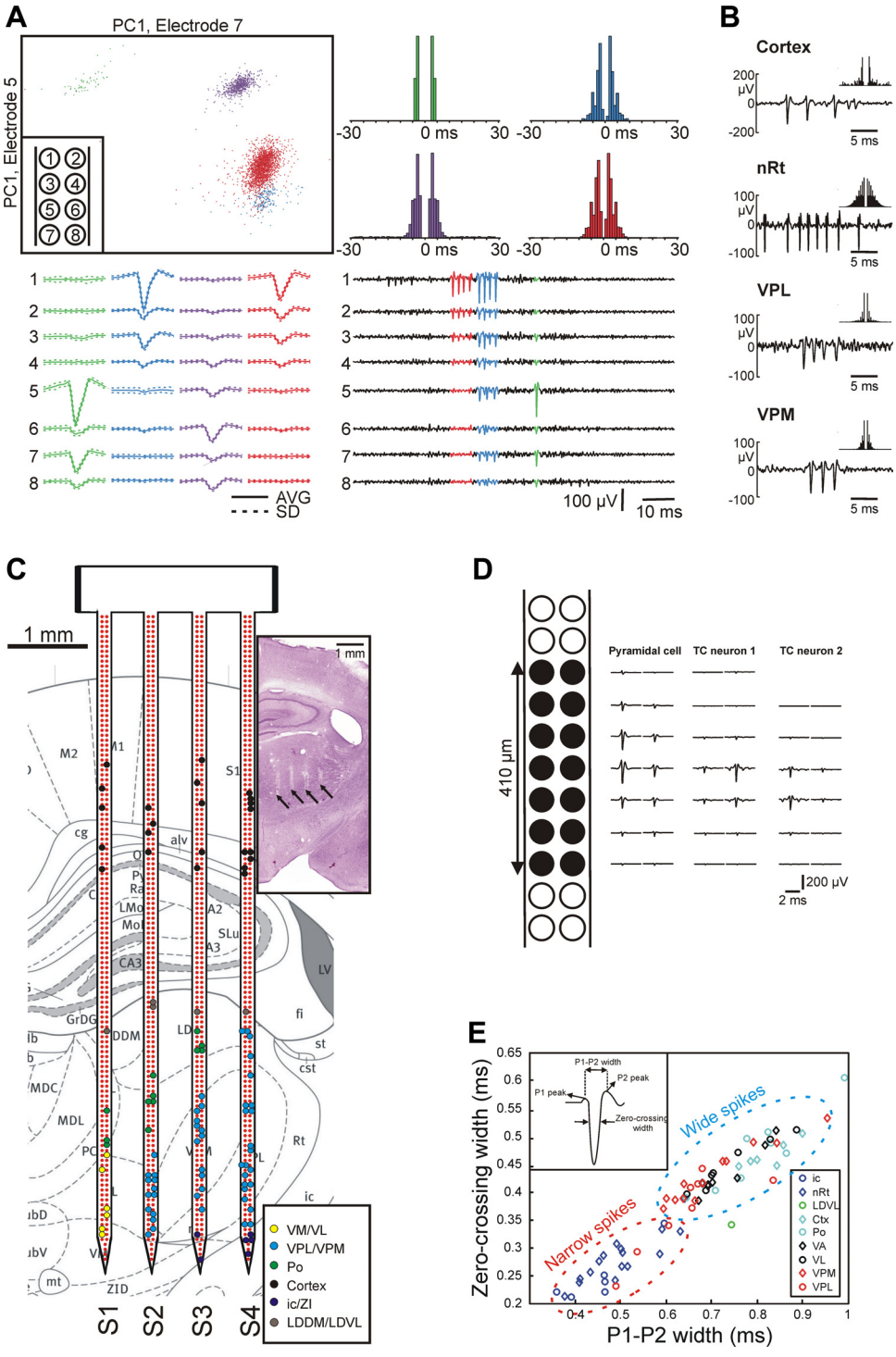

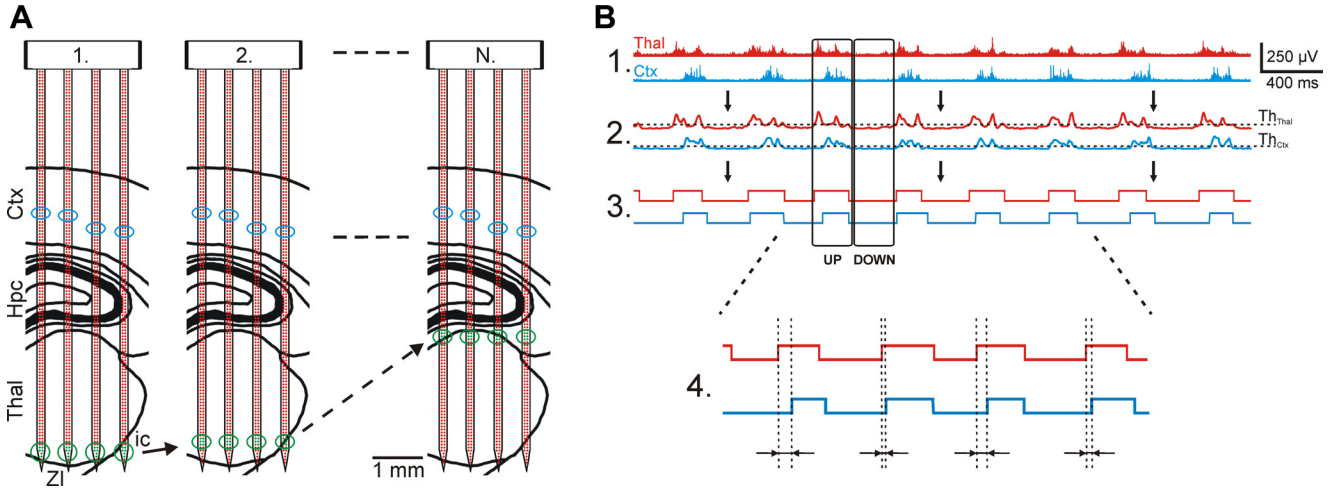

Fig. 6. Recording the thalamocortical slow-wave activity (SWA) with the EDC probe in multiple brain areas and the steps used to process the recorded data. *A*: mapping protocol used to record simultaneous activity in the thalamus and the neocortex. At least 2 recording sites on each shaft were selected in the cortex where unit activity with high SNR was detected (blue circles). The remaining recording sites were positioned near the tip of the probe, which was located in the thalamus (green circles; *1*). After a few minutes of continuous recording, these thalamic sites were repositioned to new sites in the thalamus and a new recording file was started (*2*). This procedure was continued until the whole thalamus was mapped (*N*). *B*: multiple-unit activity (MUA)-based detection of up- and down-state onsets. After the wideband data were filtered (bandpass filter, 500-5,000 Hz; *1*), the envelope of the MUA signals was obtained with a low-pass filter (30 Hz; *2*). A threshold level was calculated on each channel based on the average and SD of MUA during down-states (Th_{Ctx} and Th_{Thal}). The calculated threshold was used to acquire the up- and down-state onsets (*3*). Finally, the time difference between cortical and thalamic up-state onsets was calculated by subtracting the time point of the cortical up-state onset from the time point of the thalamic up-state onset (*4*). Thalamic traces are red and cortical traces are blue.

based localization of probe tracks and recording sites and to find the borders between different thalamic nuclei [e.g., ventral posterolateral nucleus (VPL) and ventral posteromedial nucleus (VPM), Fig. 7*C*]. Mapping thalamic nuclei with somatosensory stimulation can be done in a relatively short time. We performed the mapping by rhythmically stimulating certain body parts of the animal and verified the evoked responses by listening to the MUA frequency band on loudspeakers. After finishing with the stimulation at the actual recording location, we switched to new thalamic recording sites and repeated the same stimulation procedure.

In the representative experiment shown in Fig. 7, based on histological examinations, three of four shafts were located in the parietal association cortex (PtA), whereas the most lateral shaft was recording electrical activity from the primary somatosensory cortex (S1Tr; Fig. 7*A*). For each of the four cortical sites located on different shafts, two separate color maps were calculated that show the mean and SD of up-state onset time differences between all thalamic sites and the corresponding cortical site (Fig. 7*B*). Clear differences were seen in the up-state coupling between the cortex and different thalamic nuclei. Our results indicate that in the case of this representative experiment, the up-states were initiated, on average, earlier (~5–40 ms) in the higher order somatosensory thalamic nucleus (posterior nucleus, Po) compared with up-states detected in the cortex [Fig. 7*B*, blue color; Po vs. medial parietal association cortex (MPtA): Fig. 7, *D* and *E*]. In contrast, in the higher order visual thalamic nucleus (laterodorsal ventrolateral nucleus, LDVL), in addition to thalamic up-states being shorter in duration, these up-states also lagged behind cortical up-states with a latency of ~15–45 ms (Fig. 7*B*, yellow-red color; LDVL vs. MPtA: Fig. 7, *D* and *E*). Furthermore, we found *clear* differences between the color maps corresponding to different cortical regions (Fig. 7*B*, *color maps I—IV*). For example, when the up-state onset dynamics are compared between the VPM/VPL and the association

Fig. 5. Evaluation of the single-unit activity (SUA) recorded with the EDC probe in anesthetized rats. *A*: results of spike sorting of a representative thalamic recording showing 4 well-isolated neuron clusters. The thalamic SUA was obtained from an octrode (8 adjacent recording sites; *inset* at *top left*) of a single shaft. Clustering was performed manually in 2-dimensional feature space [*top left*; first principal component (PC1) of spikes on 2 different channels]. Neuron clusters are represented with different colors. The action potential waveforms of the isolated units can be observed on multiple channels (*bottom left*, average spike waveform; *bottom right*, 100-ms-long traces of SUA; the electrode-channel relationship is shown in the *inset* at *top left*). The autocorrelograms corresponding to the neuron clusters show burst activity with 2–5 spikes per burst (*top right*; 1-ms bin width). *B*: action potential waveforms and autocorrelograms (±30 ms, 1-ms bin width) of representative sorted neurons located in the neocortex and in various thalamic nuclei. nRt, nucleus reticularis thalami; VPL, ventral posterolateral nucleus; VPM, ventral posteromedial nucleus. *C*: all sorted thalamic and cortical single units from a single experiment (colored dots) overlaid on the anatomical map of the coronal section [adapted from the rat brain atlas, Paxinos and Watson (2007), used with permission. This was published in *The Rat Brain in Stereotaxic Coordinates*, Paxinos and Watson, Copyright Elsevier (2007).] corresponding to the Nissl-stained section containing the probe tracks (*inset*; tracks of the probe are marked with black arrows). The single units are colored on the basis of their estimated anatomical location. Dots representing individual neurons are placed over the recording site that recorded the spikes of the particular unit with the largest amplitude. Note that the anatomical map of the coronal section is not faithfully representing the real brain tissue of the investigated rat; therefore, some of the dots are not placed over the correct anatomical structure (e.g., some of the black dots, which represent cortical neurons, are located outside the cortex). *D*: 2-dimensional spatial distribution of the mean action potential waveform of a putative pyramidal cell (*left*) and 2 putative thalamocortical (TC) cells (*middle* and *right*). Spiking activity was recorded with the black recording sites indicated at *far left*. Two separate but overlapping octrode recording configurations were used to obtain the data. Note the larger potential field of the spike of the putative pyramidal cell. *E*: distribution of the P1–P2 width (*x*-axis) and zero-crossing width (*y*-axis) calculated from the mean action potential waveform of a subgroup of the sorted units. The units were recorded from different brain areas. Two distinct groups can be observed: units from the nRt (inhibitory neurons) and internal capsule (ic; axonal fibers) displayed narrow spikes, whereas the majority of the remaining neurons fired wide spikes. LDDM, laterodorsal dorsomedial nucleus; LDVL, laterodorsal ventrolateral nucleus; Po, posterior nucleus; PtA, parietal association cortex; VA, ventral anterior nucleus; VL, ventral lateral nucleus; VM, ventral medial nucleus; ZI, zona incerta.

cortices (Fig. 7*B*, *color maps I–III*) and between the VPM/VPL and the somatosensory cortex (Fig. 7*B*, *color map IV*), it is apparent that, on average, up-states in the latter cortical structure started before VPM/VPL up-states (Fig. 7*B*, *color map IV*, yellow-orange color), whereas up-states in the association cortices were initiated on average at the same time compared with thalamic up-states (Fig. 7*B*, *color maps I–III*, green color; VPM/VPL vs. MPtA: Fig. 7, *D* and *E*).

This time difference between the color maps corresponding to distinct cortical regions may indicate the propagation of slow waves in the cortex, which was described by several groups (Fucke et al. 2011; Massimini et al. 2004; Murphy et al. 2009). We found that in the coronal plane, cortical slow waves were traveling in the lateromedial direction, between the probe shafts (Fig. 8, *A* and *B*). In the illustrative example in Fig. 8, *A* and *B*, up-states started most frequently on the most lateral

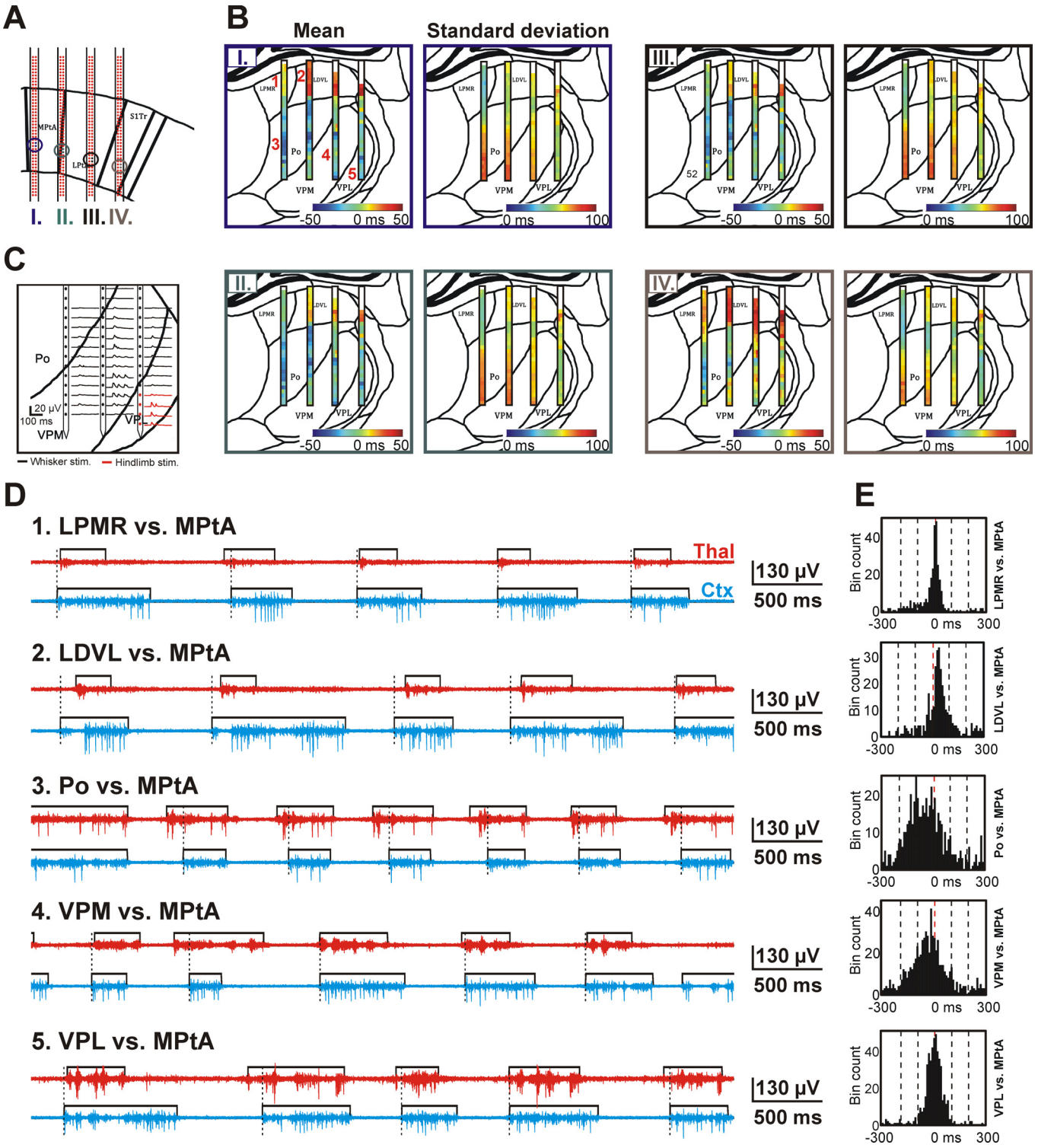

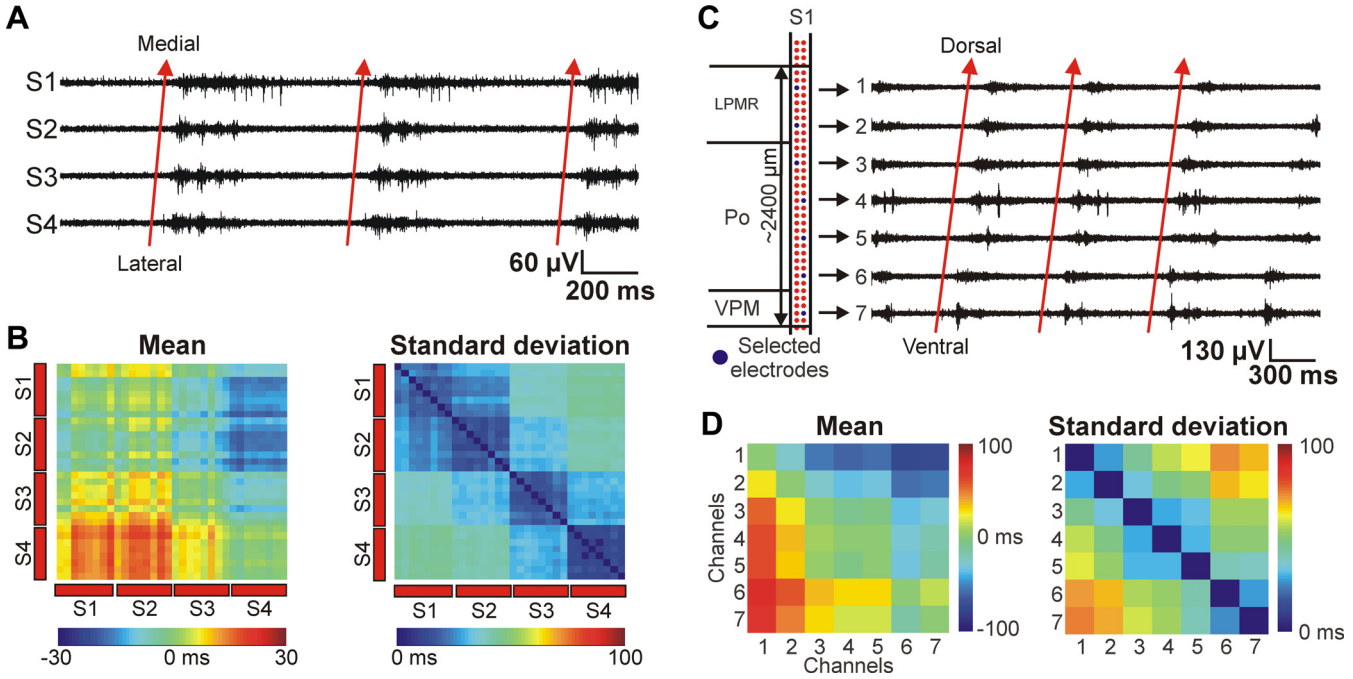

Fig. 8. Preferred cortical and thalamic propagation patterns of thalamocortical SWA under ketamine-xylazine anesthesia. *A*: 2-s-long MUA traces of 4 cortical recording sites (S1–S4) located on different shafts showing 3 consecutive up-states recorded in layer 5. The recording sites were selected near the sites indicated in panel A of Fig. 7. The up-states propagated most frequently from the most lateral shaft ('S4', primary somatosensory cortex) in the direction of the most medial shaft ('S1', medial parietal association cortex) with a latency of 10–30 ms (red arrows). B: Mean (*left*) and standard deviation (*right*) of the up-state onset time difference between up-states detected on cortical recording sites located in layer 5. The color maps were constructed from the data set of the same animal shown in *A* and in Fig. 7. However, in this case all recordings sites were selected in the cortex. On the color map of the mean up-state onset time difference, red color represents the lead of up-states detected in positions located on the *y*-axis relative to the positions on the *x*-axis. *C*: 3-s-long MUA traces showing the ventral-to-dorsal propagation of up-states detected in the thalamus (red arrows) on 1 shaft of the EDC probe. The latency between the up-state onsets detected on the most ventral and on the most dorsal electrode was greater than 50 ms. The 7 thalamic recording sites were selected in a way to be able to record from a larger volume of thalamus in the dorsoventral plane, covering several nuclei (*left*). The eighth site was located outside the thalamus. *D*: mean (*left*) and SD (*right*) of the up-state onset time difference between up-states detected on thalamic recording sites. The recording sites were selected on that shaft that was located most medially. On the color map of the mean up-state onset time difference, red color represents the lead of up-states detected in positions located on the *y*-axis relative to the positions on the *x*-axis.

shaft (*shaft 4*, S1Tr) and propagated to the most medial shaft (*shaft 1*, PtA), suggesting a preferred direction of up-state propagation from the somatosensory cortex into the association cortex.

Scientific literature investigating wave propagation in the thalamus is scarce, and these studies mainly focus on spindle oscillations (Contreras et al. 1997; Kim et al. 1995; Muller and Destexhe 2012). To the best of our knowledge, this is the first report demonstrating propagating thalamic slow waves detected in vivo in the brain of ketamine-xylazine-anesthetized rats. The propagating waves found in the thalamus partially explain the results seen on the color maps in Fig. 7, namely, the frequent early up-state onset in the Po and the delayed up-states in the higher order visual nuclei. Up-states recorded on the shaft with the most medial location most likely started near ventral recording sites and spread to dorsal thalamic positions (Fig. 8, *C* and *D*). Based on our method of up-state onset detection, almost every fourth up-state started on recording sites located in the ventral thalamus and propagated dorsally. Up-states with different propagation patterns were detected, as well, but with less frequent occurrence. It is important to note that the dynamics of thalamic slow-wave propagation are more complex than the simple example described here. The observed thalamic propagation patterns depended on several factors (not shown), for example, on the investigated thalamic areas, on the depth of the

Fig. 7. Spatiotemporal dynamics of the thalamocortical SWA observed in a representative rat. *A*: the 4 positions (1 per shaft) from where cortical recordings were obtained and used to derive the color maps shown in *B* (*I-IV*). Recording sites were located in layer 5 of association and somatosensory cortices. The relationship between the cortical sites and the color maps in *B* is color coded. *B*: color maps constructed from the mean and SD of the time difference of up-state onsets calculated between the cortical sites shown in *A* and between various thalamic sites. The color maps are representative examples from a single rat. On the color map of the mean up-state onset time difference, blue colors indicate that up-states detected on thalamic sites usually started before cortical up-states, whereas red colors represent the lead of cortical up-states. White color at the top of the color map indicates areas where no significant MUA could be detected. *C*: in addition to histological verification, the thalamic position of recording sites was also verified using somatosensory stimulation. In this representative example, repetitive (~1 Hz) whisker (black) and hindlimb stimulation (red) was applied to determine the approximate position of the borders between VPL, VPM, and Po thalamic nuclei. Evoked MUA responses on 3 shafts are shown. *D*: representative MUA traces showing the up-state dynamics between different thalamic and cortical sites. The position of thalamic sites is indicated in *B* next to the mean color map corresponding to cortical *site I* (*top left*; Arabic numerals with red color). Black rectangles show the detected up-states. The onset of cortical up-states is marked with dashed black lines. *E*: histograms of up-state onset time differences calculated between recording sites presented in *D*. LDVL, laterodorsal ventrolateral nucleus; LPMR, mediorostral part of the lateral posterior nucleus; LPtA, lateral parietal association cortex; MPtA, medial parietal association cortex; Po, posterior nucleus; S1Tr, trunk region of the primary somatosensory cortex; VPL, ventral posterolateral nucleus; VPM, ventral posteromedial nucleus.

anesthesia, or on the incoming sensory inputs perturbing the ongoing internal brain activity.

Tonotopic Mapping in the Auditory Thalamus of Rats

Besides the somatosensory network, the auditory thalamocortical system is also extensively studied (Huetz et al. 2011; Imaizumi and Lee 2014; Lee 2013; Winer et al. 2005). However, it is challenging to record simultaneously the activity of the auditory thalamus (medial geniculate body, MGB) and the auditory cortex (AC) because of the lateral location of the AC and the relatively small size of the MGB. The EDC probe could provide a good solution with its high number of closely spaced recording sites. We can identify the electrodes showing neural responses to acoustic stimulation and limit our investigations to the subset of these electrodes. In all of our experiments where the EDC probe was implanted into the auditory system ($n = 4$), we were able to simultaneously record from the auditory thalamus and cortex. This was validated by postmortem histology and by evoked MUA responses to acoustic stimulation. Figure 9*A* shows the schematic EDC probe overlaid on a Nissl-stained coronal rat brain section containing the probe tracks. In this representative example all four probe shafts penetrated the auditory cortex; one shaft was located in the dorsal division (MGD) of the MGB, whereas two shafts were found in the ventral division (MGV). The comparison of the histology and electrophysiological recordings also supported this finding. Sound-evoked MUA responses were recorded on cortical recording sites located on all four shafts (Fig. 9*A*, blue dots; Fig. 9*B*, *top*), whereas recording sites on three of the four shafts recorded sound-evoked MUA responses from the thalamus (Fig. 9*A*, blue dots; Fig. 9*B*, *bottom*). We determined the timing of neuronal responses in the different brain regions relative to the auditory stimulus. Responses in the MGB had clearly shorter MUA latencies compared with cortical MUA responses (Fig. 9*B*, dashed lines). Furthermore, as previously shown (Malmierca 2003), we found a time difference within the MGB: responses recorded from the MGV had shorter latencies than those from the MGD (Fig. 9*B*, *bottom*).

To investigate the dynamics of the thalamocortical SWA, it is necessary to examine regions in the thalamus and neocortex that are directly interconnected with each other. Because of the tonotopic organization of the rodent auditory thalamocortical system (Hackett et al. 2011; Shiramatsu et al. 2016) and the features of the EDC probe, we can find regions that are likely connected to each other (Fig. 10). Investigating the activity between such coupled areas may increase the impact and accuracy of our findings. For example, interconnected regions can be identified by constructing tonotopic color maps from the evoked cortical and thalamic MUA responses to pure tones (Fig. 10, *A* and *B*). Cortical and thalamic areas with a significant MUA response to pure tones with the same frequencies may indicate such directly coupled regions (Fig. 10*C*). Mapping of the auditory thalamus and the cortex using acoustic stimuli with the subsequent construction of tonotopic color maps can be performed relatively rapidly. After that, we can select the appropriate recording sites to investigate the thalamocortical network activity between the interconnected areas.

Large-Scale Recordings from the Mouse Brain Combined with Optogenetics

The EDC system was also applied to record the electrical activity from the brain tissue of mice (Fig. 11*A*). Genetically engineered transgenic mice are of great importance in neuroscience, especially in the field of optogenetics, where the animals are genetically modified to express light-sensitive ion channels in a labeled subpopulation of neurons (Boyden et al. 2005; Yizhar et al. 2011). During optogenetic experiments, light pulses of different wavelengths are used in the brain tissue to control the activity of neurons containing these light-sensitive proteins by either exciting or inhibiting them. Therefore, optogenetics is an excellent tool to study

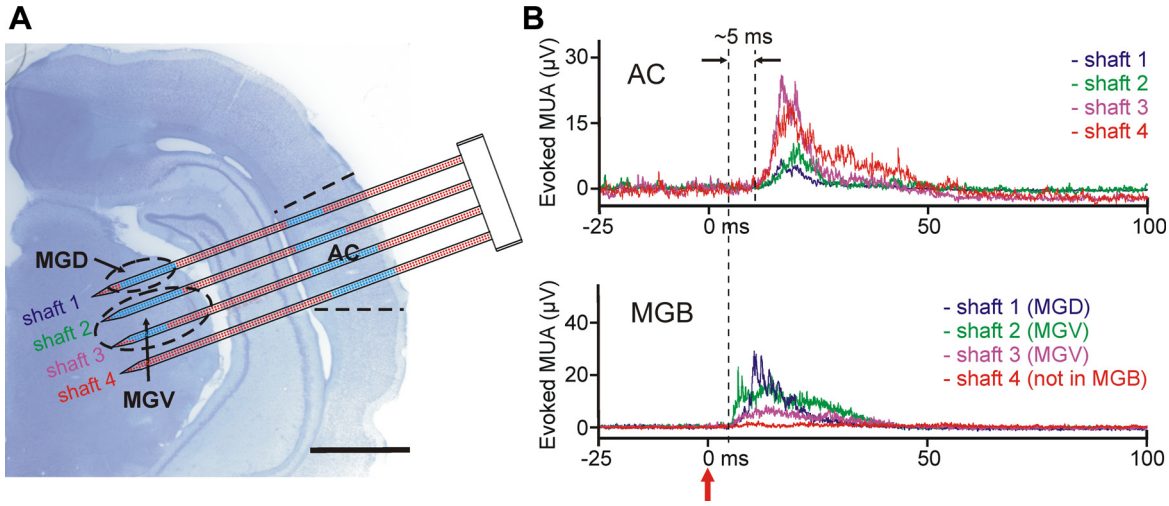

Fig. 9. Electrical activity recorded with the EDC probe from the auditory thalamocortical system of the anesthetized rat. *A*: the schematic of the probe overlaid on the top of a Nissl-stained coronal rat brain section containing the probe tracks. The shafts of the probe were located in the auditory cortex (AC) and in the ventral (ventral medial geniculate, MGV) and dorsal (dorsal medial geniculate, MGD) divisions of the medial geniculate body (MGB). To penetrate through both structures, the probe was inserted at an angle of 70° relative to the dorsoventral axis. After the implantation of the probe, click stimuli were delivered to the contralateral ear of the animal and the electrical activity was examined at every electrode position that was located in the brain, to find areas responding to sound. Blue dots show recording sites with significant MUA response to click stimuli. Scale bar, 2 mm. *B*: representative mean evoked MUA responses (averaged from $n = 20$ trials) in the AC (*top*) and in the MGB (*bottom*) to acoustic click stimulation. A single example from each shaft is presented. There was no response to sound on that part of the fourth shaft, which was located in the thalamus. The click stimulus was delivered at *time 0* (red arrow).

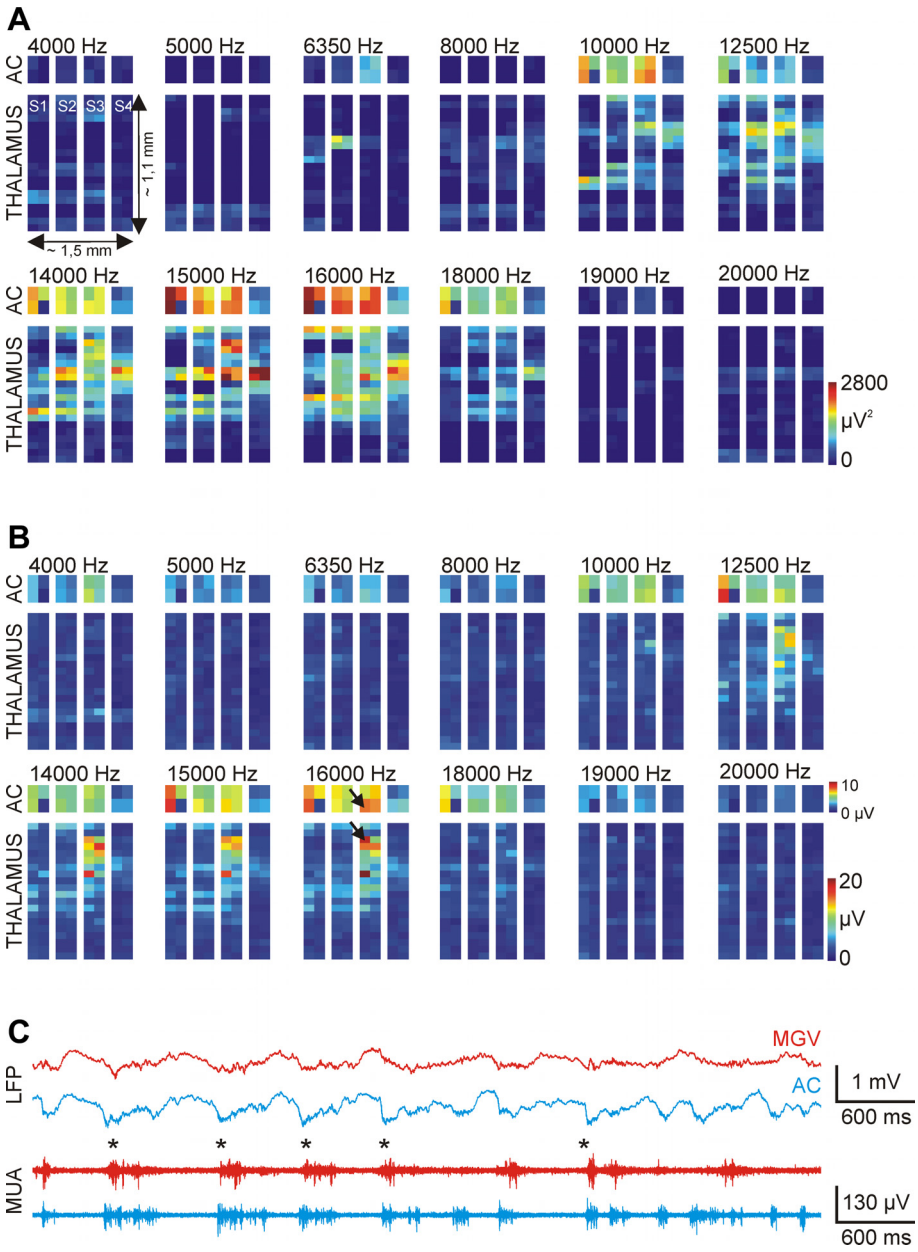

Fig. 10. Tonotopic mapping in the ventral division of the auditory thalamus of the anesthetized rat. Tonotopic maps were constructed from the integral (*A*) and the peak value (*B*) of the first 100-ms-long section of the mean evoked MUA response to acoustic stimulation (n = 20 trials). Pure tones with 12 different frequencies (4–20 kHz) were used for tonotopy. The construction of tonotopic maps was done in the following way: 4 recording sites had fixed cortical positions on each shaft, whereas the remaining 4 electrodes were located in the thalamus. After a few minutes of acoustic stimulation and continuous recording of the neural activity, thalamic sites were repositioned. Using this procedure, we could map the sound-evoked brain activity on the section of the recording probe that was located in the thalamus. *C*: local field potential (LFP) and MUA traces corresponding to a cortical and a thalamic site (indicated with black arrows in *B*) with a match in the tonotopy at 16 kHz. The asterisks indicate up-states with synchronous onset. AC, auditory cortex; MGV, ventral medial geniculate.

neuronal connectivity. However, with the electrophysiological recording techniques currently available, mapping the response of large brain regions to a given stimulus is hard to achieve.

We aimed to test the utility of the EDC probe to characterize the thalamic response after stimulating a well-studied top-down corticothalamic pathway linking layer 5 of the S1 cortex and Po (Fig. 11*B*; Groh et al. 2008, 2014). This pathway is known to be extremely efficient at low stimulation frequencies but expresses pronounced short-term depression at higher frequencies. The pathway is known to innervate Po but not VPM (Hoogland et al. 1991). In our experiments we used a transgenic mouse line (Thy-1) expressing channelrhodopsin (ChR2) in the neocortex exclusively in layer 5. The thalamic location of recording sites was determined using somatosensory stimulation and postmortem histology (Fig. 11*C*). After optogenetic stimulation of layer 5 at 1-Hz, short latency, large-amplitude responses were detected on recording sites situated mainly within Po (Fig. 11*D*; Fig. 11*F*, *top*). The response displayed hot spots consistent with the patchy nature of the L5-Po connection (Groh et al. 2014). VPM regions ventral to Po displayed very little short-latency response. After 20-Hz stimulation, the amplitude of the response displayed significant depression (Fig. 11*E*; Fig. 11*F*, *bottom*). The analysis of SUA can reveal the contribution of different thalamic neurons to responses evoked with different frequencies (Fig. 11*G*).

DISCUSSION

We have described an electrophysiological recording system comprising multishank, high-density silicon probe arrays. The recording system applies an innovative concept, the electronic selection of recording sites, which can be utilized to gather neuronal data in an effective way. The effectiveness of the

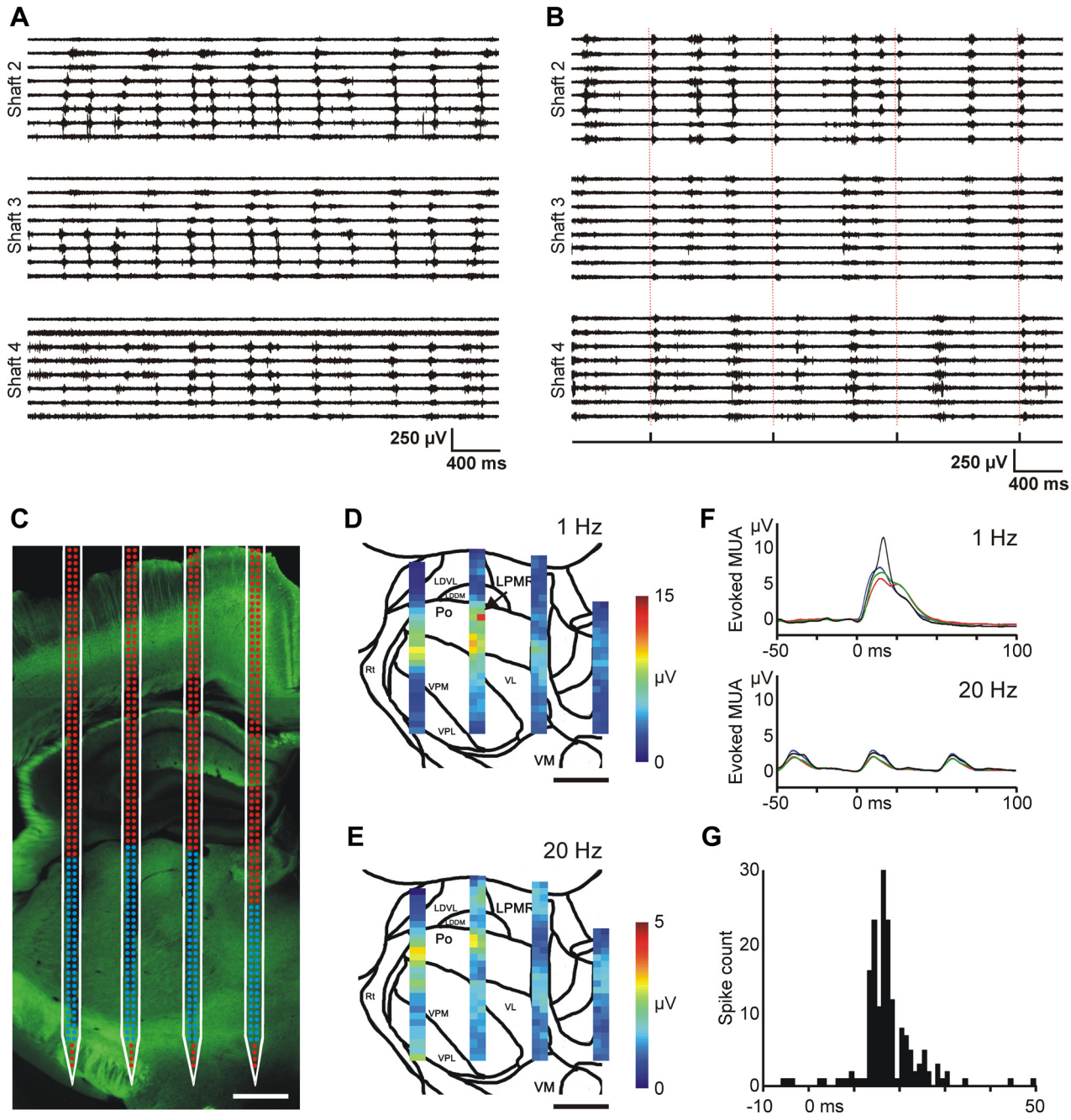

Fig. 11. Optogenetic experiments with the EDC probe in mice. *A*: 4-s-long spontaneous MUA traces recorded under ketamine-xylazine anesthesia in the mouse thalamus. Traces recorded on 3 shafts of the EDC probe are shown. Note the different propagation patterns of thalamic up-states across recording sites. The electrodes were configured in a way similar to that shown in Fig. 8*C* (expanded configuration). These propagating patterns bear a close resemblance to thalamic up-state propagation we observed in rats (see Fig. 8, *C* and *D*). *B*: 4-s-long MUA traces recorded in the thalamus of the anesthetized mouse during optical stimulation. In this case octrode configuration was used for MUA recordings. Optical stimulation of the somatosensory cortex (0.8 mW, 1 Hz) elicited MUA responses in the thalamus. The delivery times of the laser stimuli are shown on the trigger channel (*bottom*) and are also indicated with dashed red lines. Strong MUA response is present on *shaft 2* after each stimulus. *C*: fluorescent light microscopic image of the enhanced yellow fluorescent protein (EYFP) signal in the thalamus at the site of the probe penetration with the schematic of the probe overlaid on the photomicrograph. The location of the probe was estimated on the basis of the position of the probe tracks and the implantation depth. The activity recorded on electrodes with blue color was used to construct color maps shown in *D* and *E*. Scale bar, 500 μm. *D* and *E*: color maps showing the peak amplitude of the mean MUA response at every thalamic recording site in response to optical stimulation of the somatosensory cortex with 1-Hz (*D*) and 20-Hz (*E*) frequencies. Sites with no detectable MUA were excluded from the analysis. Scale bar, 500 μm. *F*: the averaged (n = 30 trials) and filtered (100 Hz, low-pass filter) MUA response to 1-Hz (*top*) and 20-Hz (*bottom*) blue light stimulation recorded on 4 adjacent electrodes. The position of recording sites is indicated with a black arrow in *D*. Optical stimuli were delivered at *time 0*. *G*: peristimulus time histogram (PSTH; optical stimuli vs. spike times) of a light-responsive thalamic single unit (bin width: 1 ms). Optical stimuli (n = 390) were delivered at *time 0*.

system has been proven in a wide range of acute electrophysiological experiments conducted in anesthetized rodents. The EDC probe performed well for recording SUA and MUA under different experimental conditions, both in the thalamus and in the neocortex. The recorded unit activity was stable for hours, with only minor changes in the spike amplitudes over time. Furthermore, the system has been successfully used to register brain electrical activity in vivo, simultaneously from multiple brain areas (which could be located several millimeters apart) and on multiple timescales (from slow brain rhythms to spikes of neurons). The high number and high density of recording sites are suitable for locating areas in the brain linked together, which in turn can facilitate the investigation of brain functions emerging from the orchestrated activity of widely distributed neural networks.

Comparison of the Electrophysiological Performance of EDC Probes and Passive Silicon Multielectrodes

Recording the electrical activity of a high number of neurons is a prerequisite for the understanding of complex coding mechanisms underlying different brain functions (Buzsáki 2004) and became feasible recently with the use of passive high-density multielectrode arrays developed over the last years (Berényi et al. 2014; Blanche et al. 2005; Lopez et al. 2014; Shobe et al. 2015). However, some of these brain functions are thought to be generated from the dynamic interaction of spatially distributed neural circuits, where the participating areas may be separated even several millimeters away from each other. For example, the process of memory consolidation is supported by several neural oscillations that appear during slow-wave sleep (Rasch and Born 2013). Numerous research studies have shown that some of these brain rhythms (thalamocortical SWA, sleep spindles, hippocampal sharp-wave ripples) are generated in widespread neural networks (Buzsáki 2015; Crunelli et al. 2015; Luthi 2014). Therefore, local recording of neuronal activity using tetrodes or single-shank silicon probes with closely spaced recording sites may be insufficient to obtain important features of the investigated brain function. The multishank EDC probe presented in this study is capable of recording neuronal activity from multiple distinct brain areas in parallel (e.g., cortical and thalamic areas of the somatosensory and auditory system) with the possibility of fine-tuning the recording positions without the physical movement of the device.

Experiments using high-channel count passive probes produce a massive amount of raw data (>10 GB/h using high sampling rates) when recording the activity on all of the electrodes, including those that were located outside the examined brain area or contained no detectable SUA. Thus a significant part of the recorded data will be inadequate for subsequent analysis. With the EDC system, we can keep the amount of recorded data reasonable by recording only from those electrodes located in brain structures of interest. Furthermore, dynamic selection of recording sites may improve the single-unit yield of experiments by finding electrodes with high-quality unit activity.

Multiple, densely placed recording sites are optimal for unit recordings and for the separation of the recorded unit activity into single-unit clusters (Blanche et al. 2005; Gray et al. 1995; Harris et al. 2000). The additional spatial information provided by multielectrode arrays can be utilized to perform a more reliable spike-sorting procedure. Furthermore, since the activity of the recording sites of the EDC probe can be manually scanned in a relatively short time (e.g., mapping with somatosensory stimulation), the features of the monitored electrophysiological signals can be used to identify different anatomical structures with high spatial precision. Consequently, the scanning may result in a more reliable identification of the target area, as well. Most of the passive silicon probes are not suited for this type of mapping, because they either have large interelectrode distances or contain recording sites confined to a small area. However, it is important to note that in the case of large structures, scanning through numerous electrodes of the EDC probe can be time-consuming.

In the case of extracellular recordings, the amplitude of the spikes of the recorded single units can significantly decrease over time (e.g., due to electrode drift) or even disappear, preventing the clear separation of the action potentials of these particular single units. In this scenario, passive multielectrodes should be moved to new positions to follow the investigated single units or to find new neurons located close to the recording sites. Unfortunately, the mechanical translation of probes increases the chance of tissue damage and bleeding, factors better to avoid during experimentation. With the use of EDC probes, new single units or areas of interest can be found by electronically selecting other recording sites, and thus we can avoid inducing further damage to the tissue around the probe.

To record brain activity from freely moving animals (especially small rodents), the recording setup (probe, base, and amplifier headstage) needs to be kept small enough to be carried by the animal on its head. In contrast, increasing the number of recording channels increases the overall recording setup size when the passive probe concept is used. However, modern CMOS technology enables the integration of electrical components, such as multiplexing and amplifying units on the probe shaft itself (Ruther and Paul 2015). The EDC system takes the advantage of CMOS technology by integrating multiplexing units on the probe shaft, thus keeping the overall recording setup size small, while having a high number and flexibility of recording channels (Dombovari et al. 2014; Lopez et al. 2014; Ruther and Paul 2015; Seidl et al. 2012; Torfs et al. 2011).

The EDC probes are suited to investigate propagating signals such as action potential backpropagation or the complex spatiotemporal dynamics of brain oscillations distributed in space. We have shown that from brain signals recorded with the EDC probe, it is possible to reconstruct the propagation patterns of the ketamine-xylazine-induced SWA in somatosensory cortical and thalamic areas of rodents with high spatial and temporal resolution. However, the drawbacks of the current system are also evident from our results. For example, the low number of simultaneously recorded sites on a single probe shaft makes current source density (CSD) analysis hard. CSD analysis, which is a widely used analysis method in experiments using passive silicon multielectrodes, reveals local transmembrane currents in a small volume of brain tissue (Mitzdorf 1985), preferably in neocortex, where the laminar structure enables the identification of current sink and source locations. The EDC probe presented in this study can have a maximum of eight recording channels in the same small volume, which

makes data recording for a reasonable CSD analysis time-consuming. We can conclude that the EDC probe is well-suited for the analysis of brain oscillation propagation between different brain areas, as well as to perform spike sorting and link the activity of clustered single cells to changes in LFP.

Current Developments and Future Applications of the EDC System

The complete system allows the simultaneous use of four multishank EDC probes, resulting in 128 recording channels in total that can be selected from a pool of more than 4,000 sites. A chronic system with flexible connections and a lightweight cable is also available, which extends the use of the system to awake behaving animals. These chronic probes with flexible cable and pointy tip were tested in one macaque monkey (*Macaca nemestrina*; L. Bononi, personal communication). The probe was implanted into the premotor cortex of the animal. The dura mater was not opened before implantation, and the pointy tip of the probe allowed it to perform the penetration and to record LFP and MUA from some of the available channels. The acute version of the probe was also evaluated by implanting it into the brain of an anesthetized head-restrained mouse placed on a spherical treadmill (F. Battaglia and T. Schröder, personal communication). During the acute experiment, the mouse was anesthetized with ketamine and the probe was implanted into the primary visual cortex. Spontaneous and flash-evoked neural activity could be recorded on several electrodes of the probe.

Further developments of the EDC probe could be a narrower shank, which might decrease the extent of tissue damage during the initial implantation and reduce brain dimpling (Sayed Herbawi et al. 2015). Smaller recording sites (10 or 20 μm in diameter) will increase the number of selectable electrodes (up to 2,000 per probe and over 8,000 electrodes in the case of 4 probes used simultaneously) and the spatial resolution of the system. Currently, we are testing probes consisting of recording sites 20 μm in diameter. Preliminary results show that the single-unit yield is higher compared with results obtained using the EDC probe with larger diameter electrodes (data not shown). In summary, the EDC system is currently well-suited for acute experiments in anesthetized rodents. However, a chronic setup for long-term electrophysiological recordings in awake and freely moving or head-restrained animals will also be available in the near future.

ACKNOWLEDGMENTS

We thank Katalin Lengyel for help during histological procedures and Péter Kottra for excellent technical assistance.

GRANTS

The research leading to these results has received funding from the European Union's Seventh Framework Programme (FP7/2007–2013) under grant agreement no. 600925 (NeuroSeeker) and from Hungarian Brain Research Program Grants. KTIA_13_NAP-A-I/1 and KTIA-13-NAP-A-IV/1-4,6. This work was partially supported by the Information Society Technologies Integrated Project NeuroProbes of the 6th Framework Program (FP6) of the European Commission under Project IST-027017.

DISCLOSURES

Arno A. A. Aarts is the CEO of ATLAS Neuroengineering. Patrick Ruther and Hercules P. Neves are co-owners of ATLAS Neuroengineering.

AUTHOR CONTRIBUTIONS

R.F., P.B., D.H., L.W., H.B., L.A., and I.U. performed experiments; R.F., P.B., D.H., L.W., H.B., and I.U. analyzed data; R.F., L.W., H.B., and L.A. interpreted results of experiments; R.F., D.H., P.R., and H.B. prepared figures; R.F. and I.U. drafted manuscript; R.F., D.H., L.W., A.A.A.A., P.R., H.P.N., H.B., L.A., and I.U. edited and revised manuscript; R.F., P.B., D.H., L.W., A.A.A.A., P.R., H.P.N., H.B., L.A., and I.U. approved final version of manuscript; A.A.A.A., P.R., H.P.N., L.A., and I.U. conception and design of research.

REFERENCES

Bai Q, Wise KD. Single-unit neural recording with active microelectrode arrays. *IEEE Trans Biomed Eng* 48: 911–920, 2001.

Barthó P, Hirase H, Monconduit L, Zugaro M, Harris KD, Buzsáki G. Characterization of neocortical principal cells and interneurons by network interactions and extracellular features. *J Neurophysiol* 92: 600–608, 2004.

Berényi A, Somogyvári Z, Nagy AJ, Roux L, Long JD, Fujisawa S, Stark E, Leonardo A, Harris TD, Buzsáki G. Large-scale, high-density (up to 512 channels) recording of local circuits in behaving animals. *J Neurophysiol* 111: 1132–1149, 2014.

Blanche TJ, Spacek MA, Hetke JF, Swindale NV. Polytrodes: high-density silicon electrode arrays for large-scale multiunit recording. *J Neurophysiol* 93: 2987–3000, 2005.

Boyden ES, Zhang F, Bamberg E, Nagel G, Deisseroth K. Millisecond-timescale, genetically targeted optical control of neural activity. *Nat Neurosci* 8: 1263–1268, 2005.

Bragin A, Hetke J, Wilson CL, Anderson DJ, Engel J Jr, Buzsáki G. Multiple site silicon-based probes for chronic recordings in freely moving rats: implantation, recording and histological verification. *J Neurosci Methods* 98: 77–82, 2000.

Buzsáki G. Hippocampal sharp wave-ripple: a cognitive biomarker for episodic memory and planning. *Hippocampus* 25: 1073–1188, 2015.

Buzsáki G. Large-scale recording of neuronal ensembles. *Nat Neurosci* 7: 446–451, 2004.

Campbell PK, Jones KE, Huber RJ, Horch KW, Normann RA. A silicon-based, three-dimensional neural interface: manufacturing processes for an intracortical electrode array. *IEEE Trans Biomed Eng* 38: 758–768, 1991.

Chen YY, Lai HY, Lin SH, Cho CW, Chao WH, Liao CH, Tsang S, Chen YF, Lin SY. Design and fabrication of a polyimide-based microelectrode array: application in neural recording and repeatable electrolytic lesion in rat brain. *J Neurosci Methods* 182: 6–16, 2009.

Cheung KC. Implantable microscale neural interfaces. *Biomed Microdevices* 9: 923–938, 2007.

Clemens Z, Molle M, Eross L, Barsi P, Halász P, Born J. Temporal coupling of parahippocampal ripples, sleep spindles and slow oscillations in humans. *Brain* 130: 2868–2878, 2007.

Contreras D, Destexhe A, Sejnowski TJ, Steriade M. Spatiotemporal patterns of spindle oscillations in cortex and thalamus. *J Neurosci* 17: 1179–1196, 1997.

Crunelli V, David F, Lorincz ML, Hughes SW. The thalamocortical network as a single slow wave-generating unit. *Curr Opin Neurobiol* 31: 72–80, 2015.

Crunelli V, Hughes SW. The slow (<1 Hz) rhythm of non-REM sleep: a dialogue between three cardinal oscillators. *Nat Neurosci* 13: 9–17, 2010.

Csicsvari J, Henze DA, Jamieson B, Harris KD, Sirota A, Bartho P, Wise KD, Buzsaki G. Massively parallel recording of unit and local field potentials with silicon-based electrodes. *J Neurophysiol* 90: 1314–1323, 2003.

Csicsvari J, Hirase H, Czurko A, Buzsáki G. Reliability and state dependence of pyramidal cell-interneuron synapses in the hippocampus: an ensemble approach in the behaving rat. *Neuron* 21: 179–189, 1998.

David F, Schmiedt JT, Taylor HL, Orban G, Di Giovanni G, Uebele VN, Renger JJ, Lambert RC, Leresche N, Crunelli V. Essential thalamic contribution to slow waves of natural sleep. *J Neurosci* 33: 19599–19610, 2013.

de Kock CP, Bruno RM, Spors H, Sakmann B. Layer- and cell-type-specific suprathreshold stimulus representation in rat primary somatosensory cortex. *J Physiol* 581: 139–154, 2007.

de Kock CP, Sakmann B. Spiking in primary somatosensory cortex during natural whisking in awake head-restrained rats is cell-type specific. *Proc Natl Acad Sci USA* 106: 16446–16450, 2009.

Delgado Ruz I, Schultz SR. Localising and classifying neurons from high density MEA recordings. *J Neurosci Methods* 233: 115–128, 2014.

DiCarlo JJ, Lane JW, Hsiao SS, Johnson KO. Marking microelectrode penetrations with fluorescent dyes. *J Neurosci Methods* 64: 75–81, 1996.

Dombovári B, Fiáth R, Kerekes BP, Tóth E, Wittner L, Horvath D, Seidl K, Herwik S, Torfs T, Paul O, Ruther P, Neves H, Ulbert I. In vivo validation of the electronic depth control probes. *Biomed Tech (Berl)* 59: 283–289, 2014.

Drake KL, Wise KD, Farraye J, Anderson DJ, Bement SL. Performance of planar multisite microprobes in recording extracellular single-unit intracortical activity. *IEEE Trans Biomed Eng* 35: 719–732, 1988.

Du J, Blanche TJ, Harrison RR, Lester HA, Masmanidis SC. Multiplexed, high density electrophysiology with nanofabricated neural probes. *PLoS One* 6: e26204, 2011.

Du J, Riedel-Kruse IH, Nawroth JC, Roukes ML, Laurent G, Masmanidis SC. High-resolution three-dimensional extracellular recording of neuronal activity with microfabricated electrode arrays. *J Neurophysiol* 101: 1671–1678, 2009.

Fiáth R, Kerekes BP, Wittner L, Tóth K, Beregszászi P, Horváth D, Ulbert I. Laminar analysis of the slow wave activity in the somatosensory cortex of anesthetized rats. *Eur J Neurosci* 44: 1935–1951, 2016.

Fucke T, Suchanek D, Nawrot MP, Seamari Y, Heck DH, Aertsen A, Boucsein C. Stereotypical spatiotemporal activity patterns during slow-wave activity in the neocortex. *J Neurophysiol* 106: 3035–3044, 2011.

Gemignani A, Laurino M, Provini F, Piarulli A, Barletta G, d'Ascanio P, Bedini R, Lodi R, Manners DN, Allegrini P, Menicucci D, Cortelli P. Thalamic contribution to sleep slow oscillation features in humans: a single case cross sectional EEG study in fatal familial insomnia. *Sleep Med* 13: 946–952, 2012.

Grand L, Pongrácz A, Vázsonyi É, Márton G, Gubán D, Fiáth R, Kerekes BP, Karmos G, Ulbert I, Battistig G. A novel multisite silicon probe for high quality laminar neural recordings. *Sens Actuators A Phys* 166: 14–21, 2011.

Gray CM, Maldonado PE, Wilson M, McNaughton B. Tetrodes markedly improve the reliability and yield of multiple single-unit isolation from multi-unit recordings in cat striate cortex. *J Neurosci Methods* 63: 43–54, 1995.

Groh A, Bokor H, Mease RA, Plattner VM, Hangya B, Stroh A, Deschenes M, Acsády L. Convergence of cortical and sensory driver inputs on single thalamocortical cells. *Cereb Cortex* 24: 3167–3179, 2014.

Groh A, de Kock CP, Wimmer VC, Sakmann B, Kuner T. Driver or coincidence detector: modal switch of a corticothalamic giant synapse controlled by spontaneous activity and short-term depression. *J Neurosci* 28: 9652–9663, 2008.

Hackett TA, Barkat TR, O'Brien BM, Hensch TK, Polley DB. Linking topography to tonotopy in the mouse auditory thalamocortical circuit. *J Neurosci* 31: 2983–2995, 2011.

Harris KD, Henze DA, Csicsvari J, Hirase H, Buzsáki G. Accuracy of tetrode spike separation as determined by simultaneous intracellular and extracellular measurements. *J Neurophysiol* 84: 401–414, 2000.

Hazan L, Zugaro M, Buzsáki G. Klusters, NeuroScope, NDManager: a free software suite for neurophysiological data processing and visualization. *J Neurosci Methods* 155: 207–216, 2006.

Henze DA, Borhegyi Z, Csicsvari J, Mamiya A, Harris KD, Buzsáki G. Intracellular features predicted by extracellular recordings in the hippocampus in vivo. *J Neurophysiol* 84: 390–400, 2000.

Hochberg LR, Serruya MD, Friehs GM, Mukand JA, Saleh M, Caplan AH, Branner A, Chen D, Penn RD, Donoghue JP. Neuronal ensemble control of prosthetic devices by a human with tetraplegia. *Nature* 442: 164–171, 2006.

Hoogland PV, Wouterlood FG, Welker E, Vanderloos H. Ultrastructure of giant and small thalamic terminals of cortical origin - a study of the projections from the barrel cortex in mice using *Phaseolus vulgaris* leucoagglutinin (PHA-L). *Exp Brain Res* 87: 159–172, 1991.

Huetz C, Gourevitch B, Edeline JM. Neural codes in the thalamocortical auditory system: from artificial stimuli to communication sounds. *Hear Res* 271: 147–158, 2011.

Ifft PJ, Shokur S, Li Z, Lebedev MA, Nicolelis MA. A brain-machine interface enables bimanual arm movements in monkeys. *Sci Transl Med* 5: 210ra154, 2013.

Imaizumi K, Lee CC. Frequency transformation in the auditory lemniscal thalamocortical system. *Front Neural Circuits* 8: 75, 2014.

Karmos G, Molnar M, Csepe V. A new multielectrode for chronic recording of intra-cortical field potentials in cats. *Physiol Behav* 29: 567–571, 1982.

Khodagholy D, Gelinas JN, Thesen T, Doyle W, Devinsky O, Malliaras GG, Buzsáki G. NeuroGrid: recording action potentials from the surface of the brain. *Nat Neurosci* 18: 310–315, 2015.

Kim DH, Wiler JA, Anderson DJ, Kipke DR, Martin DC. Conducting polymers on hydrogel-coated neural electrode provide sensitive neural recordings in auditory cortex. *Acta Biomater* 6: 57–62, 2010.

Kim U, Bal T, McCormick DA. Spindle waves are propagating synchronized oscillations in the ferret LGNd in vitro. *J Neurophysiol* 74: 1301–1323, 1995.

Kipke DR, Shain W, Buzsáki G, Fetz E, Henderson JM, Hetke JF, Schalk G. Advanced neurotechnologies for chronic neural interfaces: new horizons and clinical opportunities. *J Neurosci* 28: 11830–11838, 2008.

Kubie JL. A driveable bundle of microwires for collecting single-unit data from freely-moving rats. *Physiol Behav* 32: 115–118, 1984.

Lee CC. Thalamic and cortical pathways supporting auditory processing. *Brain Lang* 126: 22–28, 2013.

Lemieux M, Chen JY, Lonjers P, Bazhenov M, Timofeev I. The impact of cortical deafferentation on the neocortical slow oscillation. *J Neurosci* 34: 5689–5703, 2014.

Lopez CM, Andrei A, Mitra S, Welkenhuysen M, Eberle W, Bartic C, Puers R, Yazicioglu RF, Gielen GGE. An implantable 455-active-electrode 52-channel CMOS neural probe. *IEEE J Solid-State Circuits* 49: 248–261, 2014.

Luthi A. Sleep spindles: where they come from, what they do. *Neuroscientist* 20: 243–256, 2014.

Malmierca MS. The structure and physiology of the rat auditory system: an overview. *Int Rev Neurobiol* 56: 147–211, 2003.

Márton G, Kiss M, Orbán G, Pongrácz A, Ulbert I. A polymer-based spiky microelectrode array for electrocorticography. *Microsyst Technol* 21: 619–624, 2015.

Massimini M, Huber R, Ferrarelli F, Hill S, Tononi G. The sleep slow oscillation as a traveling wave. *J Neurosci* 24: 6862–6870, 2004.

McNaughton BL, Okeefe J, Barnes CA. The stereotrode: a new technique for simultaneous isolation of several single units in the central nervous-system from multiple unit records. *J Neurosci Methods* 8: 391–397, 1983.

Mechler F, Victor JD, Ohiorhenuan I, Schmid AM, Hu Q. Three-dimensional localization of neurons in cortical tetrode recordings. *J Neurophysiol* 106: 828–848, 2011.

Michon F, Aarts A, Holzhammer T, Ruther P, Borghs G, McNaughton B, Kloosterman F. Integration of silicon-based neural probes and micro-drive arrays for chronic recording of large populations of neurons in behaving animals. *J Neural Eng* 13: 046018, 2016.

Mitzdorf U. Current source-density method and application in cat cerebral cortex: investigation of evoked potentials and EEG phenomena. *Physiol Rev* 65: 37–100, 1985.

Molle M, Marshall L, Gais S, Born J. Grouping of spindle activity during slow oscillations in human non-rapid eye movement sleep. *J Neurosci* 22: 10941–10947, 2002.

Mukovski M, Chauvette S, Timofeev I, Volgushev M. Detection of active and silent states in neocortical neurons from the field potential signal during slow-wave sleep. *Cereb Cortex* 17: 400–414, 2007.

Muller L, Destexhe A. Propagating waves in thalamus, cortex and the thalamocortical system: experiments and models. *J Physiol Paris* 106: 222–238, 2012.

Murphy M, Riedner BA, Huber R, Massimini M, Ferrarelli F, Tononi G. Source modeling sleep slow waves. *Proc Natl Acad Sci USA* 106: 1608–1613, 2009.

Neves HP, Torfs T, Yazicioglu RF, Aslam J, Aarts AA, Merken P, Ruther P, Van Hoof C. The NeuroProbes Project: a concept for electronic depth control. *Conf Proc IEEE Eng Med Biol Soc* 2008: 1857, 2008.

Nguyen DP, Layton SP, Hale G, Gomperts SN, Davidson TJ, Kloosterman F, Wilson MA. Micro-drive array for chronic in vivo recording: tetrode assembly. *J Vis Exp* 26: e1098, 2009.

Nicolelis MA. Brain-machine interfaces to restore motor function and probe neural circuits. *Nat Rev Neurosci* 4: 417–422, 2003.

Nicolelis MA, Dimitrov D, Carmena JM, Crist R, Lehew G, Kralik JD, Wise SP. Chronic, multisite, multielectrode recordings in macaque monkeys. *Proc Natl Acad Sci USA* 100: 11041–11046, 2003.

Nicolelis MA, Lebedev MA. Principles of neural ensemble physiology underlying the operation of brain-machine interfaces. *Nat Rev Neurosci* 10: 530–540, 2009.

Okeefe J, Recce ML. Phase relationship between hippocampal place units and the EEG theta-rhythm. *Hippocampus* 3: 317–330, 1993.

Paxinos G, Franklin KB, Franklin KB. *The Mouse Brain in Stereotaxic Coordinates*. San Diego, CA: Academic, 2001.

Paxinos G, Watson C. *The Rat Brain in Stereotaxic Coordinates*. San Diego, CA: Elsevier Academic, 2007.

Petersen CC, Crochet S. Synaptic computation and sensory processing in neocortical layer 2/3. *Neuron* 78: 28–48, 2013.

Quiroga RQ. Spike sorting. *Curr Biol* 22: R45–R46, 2012.

Rasch B, Born J. About sleep's role in memory. *Physiol Rev* 93: 681–766, 2013.

Rey HG, Pedreira C, Quiroga RQ. Past, present and future of spike sorting techniques. *Brain Res Bull* 119: 106–117, 2015.

Robbins AA, Fox SE, Holmes GL, Scott RC, Barry JM. Short duration waveforms recorded extracellularly from freely moving rats are representative of axonal activity. *Front Neural Circuits* 7: 181, 2013.

Ruther P, Herwik S, Kisban S, Seidl K, Paul O. Recent progress in neural probes using silicon MEMS technology. *IEEJ Trans Electr Electron Eng* 5: 505–515, 2010.

Ruther P, Paul O. New approaches for CMOS-based devices for large-scale neural recording. *Curr Opin Neurobiol* 32: 31–37, 2015.

Sakata S, Harris KD. Laminar structure of spontaneous and sensory-evoked population activity in auditory cortex. *Neuron* 64: 404–418, 2009.

Saleem AB, Chadderton P, Apergis-Schoute J, Harris KD, Schultz SR. Methods for predicting cortical UP and DOWN states from the phase of deep layer local field potentials. *J Comput Neurosci* 29: 49–62, 2010.

Sayed Herbawi A, Larramendy F, Galchev T, Holzhammer T, Mildenberger B, Paul O, Ruther P. CMOS-based neural probe with enhanced electronic depth control. In: *2015 Transducers. 18th International Conference on Solid-State Sensors, Actuators and Microsystems*, Anchorage, AK, June 21–25, 2015, p. 1723–1726.

Scholvin J, Kinney JP, Bernstein JG, Moore-Kochlacs C, Kopell N, Fonstad CG, Boyden ES. Close-packed silicon microelectrodes for scalable spatially oversampled neural recording. *IEEE Trans Biomed Eng* 63: 120–130, 2016.

Seidl K, Herwik S, Torfs T, Neves HP, Paul O, Ruther P. CMOS-based high-density silicon microprobe arrays for electronic depth control in intracortical neural recording. *J Microelectromech Syst* 20: 1439–1448, 2011.

Seidl K, Schwaerzle M, Ulbert I, Neves HP, Paul O, Ruther P. CMOS-based high-density silicon microprobe arrays for electronic depth control in intracortical neural recording–characterization and application. *J Microelectromech Syst* 21: 1426–1435, 2012.

Seidl K, Torfs T, De Mazière PA, Van Dijck G, Csercsa R, Dombovari B, Nurcahyo Y, Ramirez H, Van Hulle MM, Orban GA, Paul O, Ulbert I, Neves H, Ruther P. Control and data acquisition software for high-density CMOS-based microprobe arrays implementing electronic depth control. *Biomed Tech (Berl)* 55: 183–191, 2010.

Sheroziya M, Timofeev I. Global intracellular slow-wave dynamics of the thalamocortical system. *J Neurosci* 34: 8875–8893, 2014.

Shiramatsu TI, Takahashi K, Noda T, Kanzaki R, Nakahara H, Takahashi H. Microelectrode mapping of tonotopic, laminar, and field-specific organization of thalamo-cortical pathway in rat. *Neuroscience* 332: 38–52, 2016.

Shobe JL, Claar LD, Parhami S, Bakhurin KI, Masmanidis SC. Brain activity mapping at multiple scales with silicon microprobes containing 1,024 electrodes. *J Neurophysiol* 114: 2043–2052, 2015.

Steriade M, Contreras D, Curro Dossi R, Nunez A. The slow (<1 Hz) oscillation in reticular thalamic and thalamocortical neurons: scenario of sleep rhythm generation in interacting thalamic and neocortical networks. *J Neurosci* 13: 3284–3299, 1993a.

Steriade M, Nunez A, Amzica F. Intracellular analysis of relations between the slow (<1 Hz) neocortical oscillation and other sleep rhythms of the electroencephalogram. *J Neurosci* 13: 3266–3283, 1993b.

Steriade M, Nunez A, Amzica F. A novel slow (<1 Hz) oscillation of neocortical neurons in vivo: depolarizing and hyperpolarizing components. *J Neurosci* 13: 3252–3265, 1993c.

Steriade M, Timofeev I, Grenier F. Natural waking and sleep states: a view from inside neocortical neurons. *J Neurophysiol* 85: 1969–1985, 2001.

Torfs T, Aarts AA, Erismis MA, Aslam J, Yazicioglu RF, Seidl K, Herwik S, Ulbert I, Dombovari B, Fiath R, Kerekes BP, Puers R, Paul O, Ruther P, Van Hoof C, Neves HP. Two-dimensional multi-channel neural probes with electronic depth control. *IEEE Trans Biomed Circuits Syst* 5: 403–412, 2011.

Vandecasteele M, M S, Royer S, Belluscio M, Berényi A, Diba K, Fujisawa S, Grosmark A, Mao D, Mizuseki K, Patel J, Stark E, Sullivan D, Watson B, Buzsáki G. Large-scale recording of neurons by movable silicon probes in behaving rodents. *J Vis Exp* 61: e3568, 2012.

Van Dijck G, Seidl K, Paul O, Ruther P, Van Hulle MM, Maex R. Enhancing the yield of high-density electrode arrays through automated electrode selection. *Int J Neural Syst* 22: 1–19, 2012.

Wilson MA, McNaughton BL. Dynamics of the hippocampal ensemble code for space. *Science* 261: 1055–1058, 1993.

Winer JA, Miller LM, Lee CC, Schreiner CE. Auditory thalamocortical transformation: structure and function. *Trends Neurosci* 28: 255–263, 2005.

Wise KD, Angell JB, Starr A. An integrated-circuit approach to extracellular microelectrodes. *IEEE Trans Biomed Eng* 17: 238–247, 1970.

Wise KD, Sodagar AM, Yao Y, Gulari MN, Perlin GE, Najafi K. Microelectrodes, microelectronics, and implantable neural microsystems. *Proc IEEE* 96: 1184–1202, 2008.

Yip S, Ip JK, Sastry BR. Electrophysiological actions of hemoglobin on rat hippocampal CA1 pyramidal neurons. *Brain Res* 713: 134–142, 1996.

Yizhar O, Fenno LE, Davidson TJ, Mogri M, Deisseroth K. Optogenetics in neural systems. *Neuron* 71: 9–34, 2011.